THESIS

# DEVICE CHARACTERIZATION ON ENERGY DESIGN AND SCOPING TOOL FOR DC DISTRIBUTION SYSTEMS AND A STUDY ON HARMONICS IN AC/DC CONVERTERS IN LOW VOLTAGE DISTRIBUTION

Submitted by

Arthur Felício Barbaro dos Santos

Department of Electrical and Computer Engineering

In partial fulfillment of the requirements

For the Degree of Master of Science

Colorado State University

Fort Collins, Colorado

Summer 2020

Master's Committee:

Advisor: Peter Young

Daniel Zimmerle
Siddharth Suryanarayanan

# ABSTRACT

DEVICE CHARACTERIZATION ON ENERGY DESIGN AND SCOPING TOOL FOR DC DISTRIBUTION SYSTEMS AND A STUDY ON HARMONICS IN AC/DC CONVERTERS IN LOW VOLTAGE DISTRIBUTION

DC appliances have resurged with the evolution of power electronics and their massive application in Miscellaneous Electric Loads. The increase of DC distributed generation and battery storage has also helped boost the scientific community's attention to this other alternative. This work collects consumption data from appliances and converters connected to an AC distribution. The appliances that are focused on in this study are called Miscellaneous Electric Loads (MELs), which comprise all electronic loads in a building that are not related to lighting, heating, and air conditioning. The harmonics of these devices are analyzed in this paper as part of a relevant project funded by the Department of Energy of the United States: the Energy Design and Scoping Tool for DC Distribution Systems.

This work also presents results from another study, still within the scope of the same project, which aims to collect power consumption data on appliances commonly found in an office environment (laptop, screens, desktops, phone chargers, and network devices) over a period of approximately two months. This data will give a real estimate of these appliances' AC/DC converter operating range regarding their rated power and will allow a more complete analysis of the emission of harmonics in the power system and a comparison of harmonic cancellation in low voltage distribution systems versus the total cancellation potential.

# ACKNOWLEDGEMENTS

I would like to thank Dr. Peter Young for being my advisor and so supportive, and Dr. Sid Suryanarayanan for his great lessons and for serving on my committee.

To Daniel Zimmerle, I thank him for his mentorship and example of leadership, which has always encouraged me and kept me motivated. His deep knowledge of engineering and his practical sense was an inspiration and great incentive during this journey. I am grateful for all the opportunities he has given me, inside and outside the academy.

To Jerry Duggan, I thank him for his kind supervision, and for creating such a positive environment for learning. Throughout his guidance, he was always patient and extremely helpful since the beginning and introduced me to important skills that will have a lasting effect on my research work and career.

These are people who changed my journey and contributed immensely to my personal development and I will always owe my eternal gratitude.

To all relatives and friends who in one way or another shared their support and some special thanks to colleagues in the laboratory. To Chris, for his friendship, and the countless support at the Powerhouse. To Dr. Cale for the knowledge transmitted and assistance with laboratory tests. To Avpreet, project partner, for his friendship and assistance.

I also thank Professor Marcos Fernando dos Santos for being an example of professionalism, a key player during my academic journey, and always so helpful.

I thank my beloved parents, Rogério and Sandra, responsible for all my achievements, for their unconditional and endless support, and my sister Bárbara for the incentives. Last but not least, I thank my faithful life partner Roberta, who embarks with me on the greatest challenges, which at her side always turn into the best adventures.

# DEDICATION

*To my parents, Rogério and Sandra.*

TABLE OF CONTENTS

LIST OF TABLES

LIST OF FIGURES

# LIST OF ACRONYMS

**AC** Alternate Current

**CLB** Controllable Load Bank

**CSU** Colorado State University

**CUT** Converter Under Test

**DC** Direct Current

**DF** Diversity Factor

**DOE** Department of Energy of the United States

**FFT** Fast Fourier Transform

**HVAC** Heating, Ventilation, and Air Conditioning

**HVDC** High-Voltage Direct Current

**IQR** Interquartile Range

**LCD** Liquid Crystal Display

**LED** Light Emitting Diode

**MELs** Miscellaneous Electric Load

**MFRP** Maximum Fraction of Rated Power

**MOSFET** Metal-Oxide-Semiconductor Field-Effect Transistor

**MU** Keysight 34980A multi-function measuring unit

**NREL** National Renewable Energy Laboratory

**PA** Keysight Power Analyzer PA2203A

**PFC** Power Factor Correction

**SCPI** Standard Commands for Programmable Instruments

**THD** Total Harmonic Distortion

**THDI** Current Total Harmonic Distortion

**THDV** Voltage Total Harmonic Distortion

# Chapter 1

# Introduction

## 1.1 DC Loads and Distribution

systems have been the standard for electricity transmission and distribution, due to the ease of voltage level conversion using transformers. However, advances in power electronics have made voltage conversion in DC devices possible and inexpensive and increased the fraction of DC loads in people's daily lives. Along with the high penetration of renewable systems, these are some of the main factors that have motivated the reappearance of DC power systems and have lead to the rapid growth in its application, whether it is in power generation, transmission, distribution or consumption.

The implementation of DC systems has increased considerably in buildings, telecommunications, and has been shown to be more efficient, reliable, and economic, and to use less space than conventional AC in some cases [1–4]. Some small microgrids also benefit from DC distribution, particularly those located in rural areas, where electrical charges such as LED lights, phone chargers, and radios – all internally DC – are the predominant loads [5]. In distributed generation,solar photovoltaic systems and most energy storage systems also operate in DC. However, DC systems still need to overcome challenges, particularly in standardization and market inertia, which have impeded the production of large numbers of devices directly powered by DC rather than by local AC/DC converters.

In transmission systems, high voltage direct current (HVDC) lines have proven advantageous in certain long-distance power transmission implementations. Hydroelectric power generated at the Itaipu Dam, for example, is transmitted from Paraguay (50Hz) to Brazil (60Hz) and is a good alternative for dealing with the different grid frequencies [6].

HVDC can also be advantageous for long distances, compared to AC transmission lines, and can improve security, resiliency, and more [7].

Studies have been also analyzed the pros and cons of direct and indirect effects of DC distributions systems for commercial buildings. The Department of Energy of the United States (DOE) is currently funding research in this area, including this thesis and the studies associated with it [8,9].

This study is focused on miscellaneous electrical loads (MELs), which are devices that consume electrical energy in a building and are not associated with core functions (HVAC and lighting), like coffee makers, computers, cell phones, microwaves, etc. These MELs operate internally in DC, but are powered in AC, generating conversion losses that might be lower if these devices were operating directly in DC. Therefore, DC distribution systems may be of interest.

Different architectures have been described for AC and DC distribution systems, across a range of voltage levels [10–13]. These systems should be able to provide power with high efficiency, be reliable, and operate at low cost. Aspects that can define the topology of the system are the voltage levels, power quality, power rating and system lifespan.

The advancements in power electronics allowed high efficiency when converting the AC grid power into DC, including integration of internally-DC local generation and storage. However it would also be possible to distribute electricity in buildings using DC, by converting into the desired voltage level, an distributing via a (currently un-standardized) DC distribution network.

There are two types of DC distribution systems. The first is the unipolar system, which is a DC system with two conductors (positive and negative) and therefore has only one voltage level for the consumers. The other is the bipolar distribution system, which uses three conductors (positive, negative and neutral) providing different voltage levels [14–16]. In some scenarios, bipolar DC distribution provides more options for power conversion, increasing system efficiency, although it requires increased capital cost.

Overall losses of DC distribution system are estimated to be lower since it wouldn't need to have many conversion stages. Recent work comparing AC to DC distribution networks [17], indicates that DC distribution systems at 380VDC in data centers can save 7% and 28%, respectively, compared to the same system running in 415VAC and 208VAC.

In DC distribution systems coupled to AC systems, there are at least two conversions present: one in the distribution transformer and the other in a central AC/DC rectifier [18]. Studies show that DC distribution for commercial buildings have 12% expected savings, with potential to go up 18% [19]. The efficiency of a DC distribution system varies according to the efficiency of the converters used, the voltage level and the topology of the system (local generation, distribution transformers, etc.).

A study performed by Lawrence Berkeley National Laboratory analyzed DC-ready appliances in the market and compared their efficiency with similar AC appliances. After analyzing LED TVs, refrigerators, LEDs lamps, air conditioners and ceiling fans, all DC products were substantially more efficient than their AC equivalent [20]. Stippich et al. [21] converted a PC power-supply, a screen monitor and an LED bulb, among other devices, to DC, and were able to achieve 4.50%, 2.70%, and 15.4% energy savings, respectively. Moreover, converting appliances to high-efficiency DC technologies can save up to 30% in residential electricity consumption [22].

## 1.2 AC Harmonics from AC/DC Converters

When the impedance of a load changes with the applied voltage, we call it a nonlinear load. Therefore, if a sinusoidal voltage waveform is applied to it as the load is varying, the current will be distorted and not a perfect sinusoidal waveform. The current waveform has harmonics which, by interacting with the impedance of the distribution system, causes voltage distortion, power losses, and reduces the efficiency and power quality of the system, affecting the end consumers [23].

AC/DC converters are switch-mode power supplies and are non-linear loads, creating high current harmonics. The amount of generated harmonics varies with the power level of the power supply. With the rapid increase of MELs, the usage of converters is escalating and today it is responsible for a substantial portion of harmonic generation in commercial buildings.

High harmonic levels have significant influences in transformers and protection equipment, causing extra heating that reduces their lifespan. Additionally, it can cause protection failures that may lead to unnecessary circuit breaker trips, metering errors, and increase winding losses in distribution transformers [24].

A study showed that 3rd and 5th order harmonics are predominant in residential feeders [25]. Since residential service transformers have both sides grounded, harmonics are propagated into the medium voltage distribution system. Commercial and industrial systems generally use a three-phase delta-wye transformer that is able to trap triple harmonics [26]. Hence, while residential consumers have higher impacts on harmonics at the feeder level, it primarily affects transformers in commercial and industrial distribution systems. Gomez et. al found a quadratic relation between the distribution transformer life reduction and total current harmonic distortion (THDI). Using constant values for THDI in a simulation, they estimated that levels of THDI in the system should be below 30% to maintain a reasonable lifespan of the transformer [27].

Current harmonics could lead to voltage harmonics and overloading neutral wires, which increases both safety risks and probability of system failure [28]. Harmonics may also induce voltage on telephone lines, impacting telecommunication systems.

To deal with this problem and improve the system power quality, several techniques have been applied to cancel or mitigate harmonics. One technique is the use of phase shifting transformers, where part of the harmonics generated in the system are shifted 180 degrees, and when they are combined with others they are canceled [29]. Other resources for mitigation are connected line reactors, power factor correction (PFC), and cur-

rent shaping [30, 31]. Balcells and Garcia showed in a simulation that shunt active filters were able to decrease not only THDI but also neutral currents [32].

PFC is a widely used technique that decreases the harmonic components by increasing the power factor of the power supply. Pulses of high current and short duration are smoothed by passive or active techniques, causing the input current to decrease, and consequently the apparent power and the power factor.

Switching power supplies can be divided into three groups: No PFC, active PFC, and passive PFC [33]. When compared with equipment without PFC or with active PFC, studies indicate that appliances with passive PFC have better harmonic cancellation [34]. Technological advances have impacted current harmonics from some devices. As an example, in the 1990s, electric vehicle chargers had an average THDI of 50% back, while current models have THDI averaging 7.5%, below the limit of 17.3% established by IEC 61000-3-4 norm [30].

When there are several devices that generate harmonic components in the system, the total harmonic is not simply the arithmetic sum of all the components, as there are two effects that reduce the resulting value: the attenuation effect and the diversity effect [35].

The attenuation effect is the decrease in both magnitude and angle of the load current harmonics caused by an increase of voltage distortion [36, 37]. The diversity effect is caused by the different variety of appliances connected in the network. Their different topologies generate harmonics with different magnitudes and phase angles. Due to the phase angle diversity, when the phasor sum of all components is done, the final value is lower then the simple arithmetic sum, which neglects the phase angles [38,39]. Therefore, by dividing the phasor sum by the arithmetic sum we have the Diversity Factor (DF), which is used to estimate the harmonic cancellation in the system.

Current harmonic cancellation plays a significant role in the voltage distortion of the distribution system. As more current harmonics are canceled, the potential for voltage distortion is also reduced. Studies indicate that the attenuation effect is accentuated in

higher-order harmonics, and cancellation tends to increase with the number of devices connected to the same network [33, 40–42].

Past studies on harmonic cancellation typically assume the AC converters are working in almost their entire power range, typically from 20%-100% [36, 43–47]. These studies did not analyze the realistic operational power range of converters – i.e. the power range actually utilized on a routine basis. Therefore, if AC/DC converters are seldom utilized over their entire power range, cancellation analyses assuming use of the entire power range may be in error. In this paper, the power range of a group of appliances is collected over a period of time, and the DF is calculated for different scenarios with converters operating in realistic conditions.

## 1.3 Energy Design and Scoping Tool for DC Distribution Systems

The work described here is part of a larger study to develop a DC Design and Scope Tool that would allow building designers (architects and engineers) to compare the efficiency and cost of DC power distribution with conventional AC power distribution within commercial buildings.

The project was funded by the DOE and is being developed by a partnership between the National Renewable Energy Laboratory (NREL), CSU, Lawrence Berkeley National Laboratory (LBNL), PVI Construction Management, and partner companies. The specific aim of this project is to understand possible energy savings from powering MELs on DC distribution systems rather than using AC power distribution and local AC/DC converters.

The study-developed "DC Design Tool" will be a module of OpenStudio, a building energy simulator, and will include both life-cycle cost analysis and interoperability with the OpenStudio Building Component Library (BCL). With the power distribution system modeling, it will be possible to identify opportunities for DC power distribution, with the

aim of assessing the benefits and drawbacks of AC, DC, and hybrid distribution systems [48,49].

Within this study, the author was responsible for performing device characterization, including converter efficiency and harmonics, and comparing the efficiency of appliances powered either by AC/DC or DC/DC converters for the same load. This work presents the data from devices testing and the development of the necessary testbeds. All testing was performed at CSU's Powerhouse Energy Campus in Fort Collins, Colorado, USA.

## 1.4 Study Design and Aims

This study focuses on MELs commonly found in an office environment, testing a range of laptop computers, phone chargers, screens, desktops and network devices – all internal DC devices operating at 120VAC powered by point-of-use AC/DC converters. For external AC/DC converters, a controllable load bank was developed in the laboratory to test converters, measuring harmonics and efficiency points, across a full range of power levels, while only harmonic measurements could be made for internal AC/DC converters. While the study looked at both the efficiency and current harmonics from these devices, this work will focus on the current wave forms and harmonics at different power levels.

Since the primary hypothesis of this work is that harmonic cancellation would vary with the load level of MELs on a circuit, the study also recorded actual power consumption over a period of approximately two months for a variety of appliances (27 in total) using smart plugs. The data collected provides data to estimate where on the efficiency curve the devices most often operate and what the THDI is at those levels.

The first aim of this work is to provide the detailed description of how the testbed and the controllable load banks were implemented, which allowed the simplified data collection for the development of the DC Design and Scope Tool. The second is the analysis of current harmonic cancellation in a realistic scenario, where converters are operating in

real-world conditions, and a different quantities of appliances are connected in parallel in an AC low voltage distribution system.

## 1.5 Document Structure

This thesis is structured as follows:

Chapter 2 describes the physical assemblies necessary for testing, including both measurement equipment and device loading methods. The chapter also outlines which appliances and converters were tested and how the data were post-processed.

Chapter 3 discusses long-term recordings made to understand the frequency and characteristics of loading on AC/DC converters of certain appliances. Power consumption of each appliance was recorded at the AC system connection using smart plugs. Since these plugs had a non-trivial time constant which impacted the recorded power levels, methods to correct for this time constant are also discussed.

Chapter 4 focuses on the current harmonics generated by these tested devices in an AC distribution network. The chapter presents specific data for each group of tested devices. Finally, a simulation was performed with real data from converters to estimate real and potential harmonic cancellation in a AC distribution system.

Chapter 5 discusses the principal conclusions from this work, and suggestions for future work.

# Chapter 2

# Device Characterization

A testbed was constructed to characterize appliances and converters for the study. In addition, to build the efficiency curve for AC/DC and DC/DC converters, three controllable load banks (CLBs) were developed to assist in the automation of tests. This chapter describes the testbed construction, design, construction and operation of the load banks, and covers the equipment that was used for data collection.

Some AC/DC *external* converters, like laptops chargers, phone chargers, and etc., have easily accessible input and output ports that can be readily accessed to collect data about input harmonics and input and output power to support the calculation of efficiency curves. Others – *internal* converters – are inside of appliances, often soldered into complex electronic boards, and not readily accessible for measurement. Internal converters are common in work stations and computer screens. For these converters it is only possible to collect data on input signal harmonics.

Therefore, the device characterization can be divided in two groups: converter characterization, for the cases where we have *external* converters, and appliance characterization, when we have *internal* converters.

## 2.1 Testbed

The need to create a testbed arose at the beginning of the DC Design and Scoping Tool project, to support quantitative and qualitative analysis of different electrical load models and to test the integration of those models into the DC Design Tool. The testbed simulates energy consumption conditions similar to those found in a small commercial office building, where loads can be powered on either AC or DC. The testbed was configured to allow measurements to be compared to the results of the simulation results to check the model accuracy.

Figures 2.1 and 2.2 show conceptual configurations that were run in the testbed. The first, Figure 2.1 simulated a small office operating with an AC distribution, and the second, Figure 2.2, the same small office operating with DC distribution.

The AC distribution system is intended to emulate a commercial building distribution system, at a small scale. Primary power distribution in commercial buildings in the USA is generally performed utilizing 3-phase, 480V, distribution for large buildings or 3-phase, 208V, distribution for smaller buildings, both tied directly to the secondary of the utility distribution transformer via a power distribution panel. The test setup for this project utilizes th 3-phase, 480V, wye power distribution of the Powerhouse Energy Campus main building. The test distribution system is connected via a 3kVA delta-wye transformer (ACME model T2A533081S), with the primary connected to the utility mains using a delta connection and the secondary configured as a wye-connection with grounded neutral.

The transformer secondary feeds a typical commercial building load center, with six circuits: Four single-phase 120V, one single-phase 208V phase-to-phase, and one 208V three-phase circuit. Each 120V volt branch has 4 outlets and the single-phase and three-phase 208V circuits each have one outlet.

The load center and the 6 circuit branches were constructed on a plywood board. Each branch has a measurement box, which breaks out the respective circuit and provides measurement points for voltage and current.

Inside the load center there are 10A fuses for each of the secondary phases (a, b, and c), and each circuit has its own circuit breaker.

A testbed schematic example is depicted in Figure 2.3, representing an experiment being conducted in the AC configuration. Figure 2.4 shows a picture of this experiment.

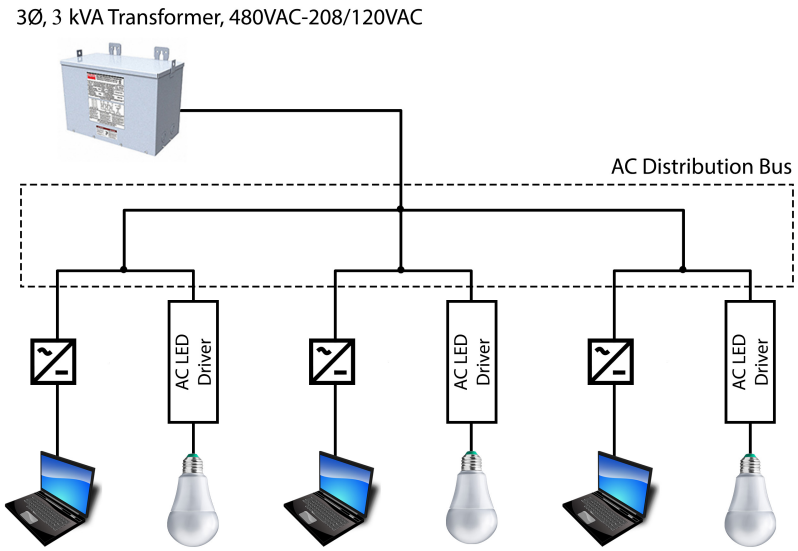


**Figure 2.1:** Conceptual diagram of the AC Testbed configuration.

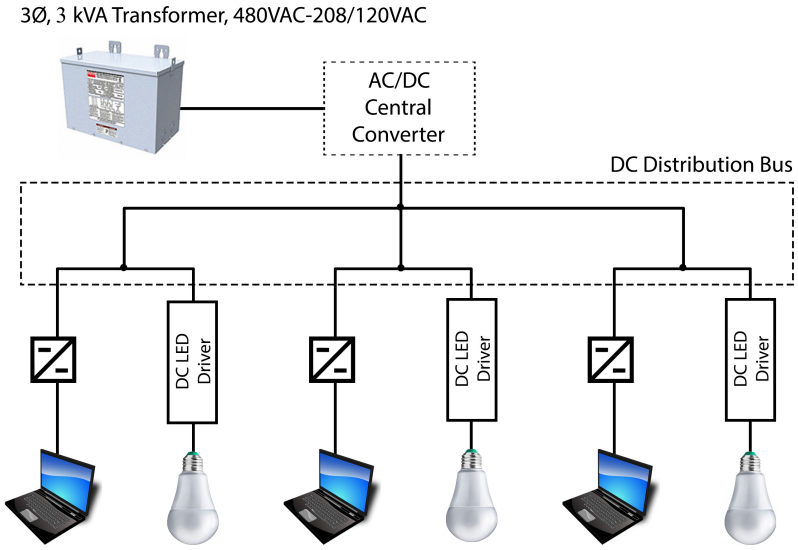


**Figure 2.2:** Conceptual diagram of the DC testbed configuration.

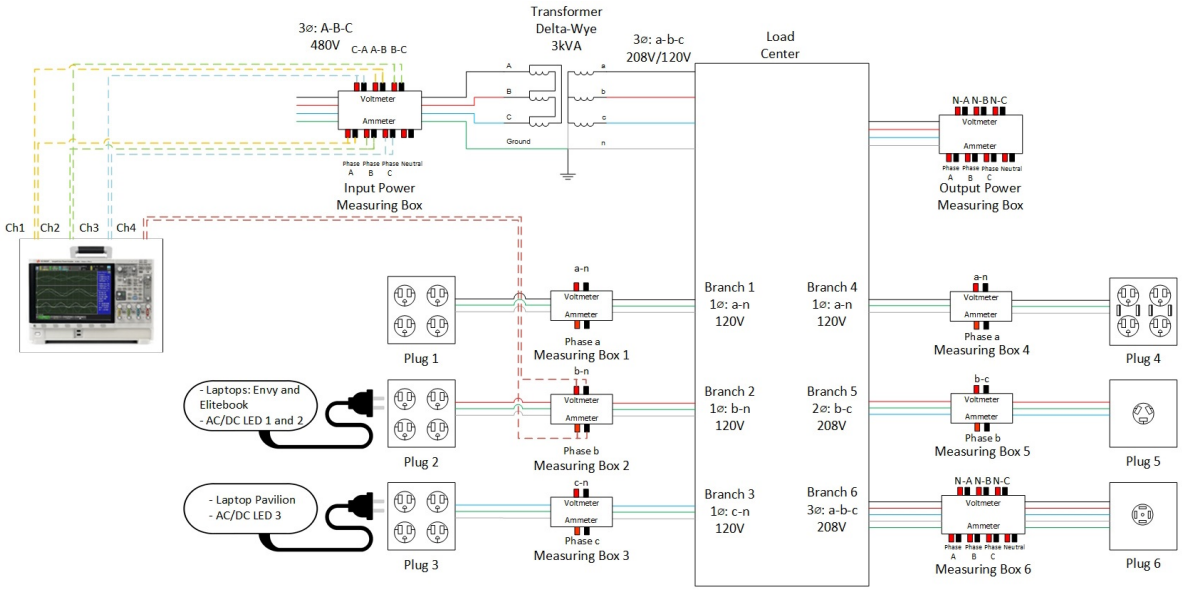


**Figure 2.3:** Schematic of the testbed illustrating all connections for the test in Figure 2.4. Measurement boxes have taps for the voltage and current probes of the power analyzer (left). Loads are connected utilizing industry standard plugs and the device's power cord.

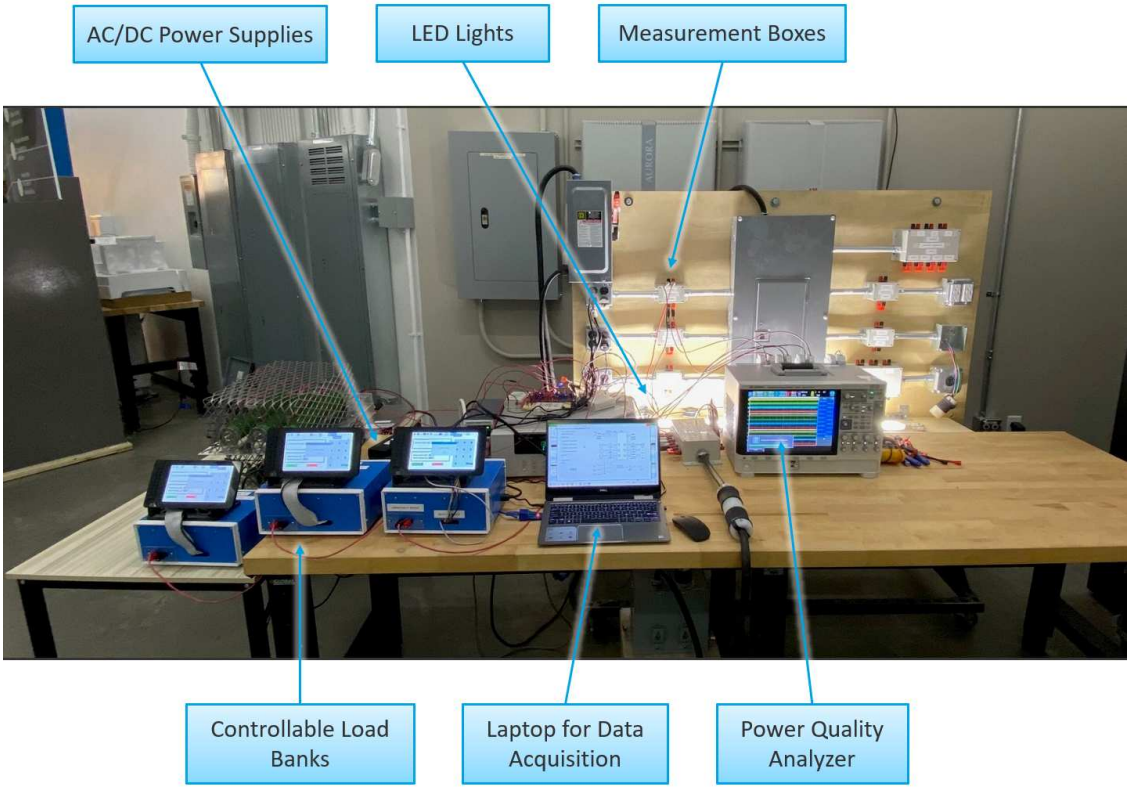


**Figure 2.4:** Experiment being conducted on the AC testbed. The experiment is configured as shown in 2.3.

## 2.2 Controllable Load Banks

Depending on the load on the converter, both current harmonics and the converter efficiency will change. Hence, to be able to analyze and compare the effects of AC and DC distribution systems, the converters/appliances needed to be loaded at a range of loads to simulate power levels seen in operational practice. To test the converters, load banks were used to vary the load applied to the converter under test (CUT). The load applied to the CUT was varied between no load (0 W) and the rated power of the CUT in 10 evenly-spaced load steps.

Different load banks were used depending on the power rating of the converter. For converters rated above 400W, experiments used the Chroma Programmable AC/DC Load Bank, model 63803, rated at 3.6 kW, with maximum voltage of 350V and current of 36A. However, since most consumer and office's power electronics are rated below 400W, dedicated controllable load banks (CLBs) were developed to load the DC side of the converter. The CLBs were rated at 400W and a maximum voltage of 20V.

Each CLB was constructed in its own 250 x 190 x 110 mm metallic case. Each CLB contained 10 resistors, mounted on two aluminum plates, with a heat sink attached underneath each plate. Chassis-mount resistors with the power rating ranging from 25-100W were used. A cooler (fan) was installed to increase air flow and thermal paste was used between the aluminum plates and the heat sinks, and between the resistors and the plates, to improve heat dissipation.

The load bank design approximated a binary pattern of resistance levels with 8 binary digits of resolution. Since resistors are only available in standard sizes, binary steps were approximated. Since commercial values of 32Ω and 64Ω were not available, 33Ω resistors were used instead. Therefore, one aluminum plate held 2Ω (2, 4Ω resistors in parallel), 4Ω, 8Ω and 16Ω resistors, while the other plate held 33Ω, 66Ω (2, 33Ω resistors in series), 128Ω and 256Ω resistors. Figure 2.5 shows the resistance values and interconnections.

After mounting the plates, the resistors were installed in the inside of a metallic case and connected to a 8-channel relay board.

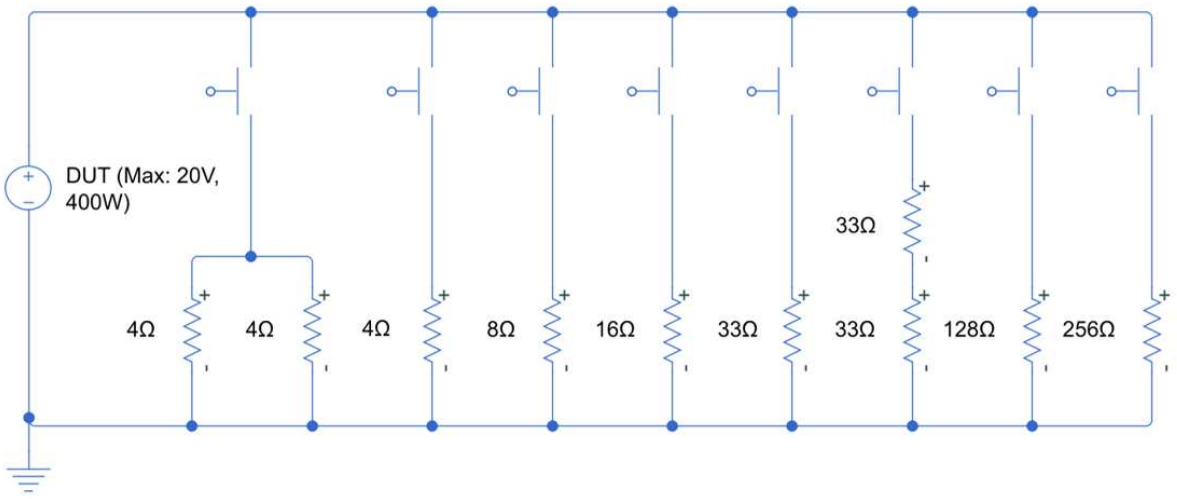


**Figure 2.5:** Controllable Load Bank Resistors Schematic.

The relay board is powered by a 12VDC AC/DC power supply, which also supplies power to two 12VDC to USB-5VDC converters: one powers a Raspberry Pi (RPi) 3+ installed on the top of the metallic case, behind a 7" LCD screen (SmartPi Touch); and the other feeds the cooler installed on the side of the case. Lastly, a ribbon cable was used to connect the relay board to the Raspberry Pi's control pins. The CUT was be connected via a pair of banana plugs in the front panel of the CLB. Figures 2.6 shows the manufacturing of one CLB and after it was built.

Relays were controlled by a Python program running on the Raspberry-Pi microcontroller. The microcontroller is connected to an LCD screen with a graphical user interface, for the user to insert the values for the CUT's voltage and rated power. The graphical user interface (GUI) was developed in Python, using the module tkinter; this program can be found in Appendix of this thesis. The GUI asks for the power analyzer's IP address, the converter's rated power and output voltage. As soon as the "Run" button is hit, the RPi calculates the appropriate values of resistance needed to perform the load steps. For ex-

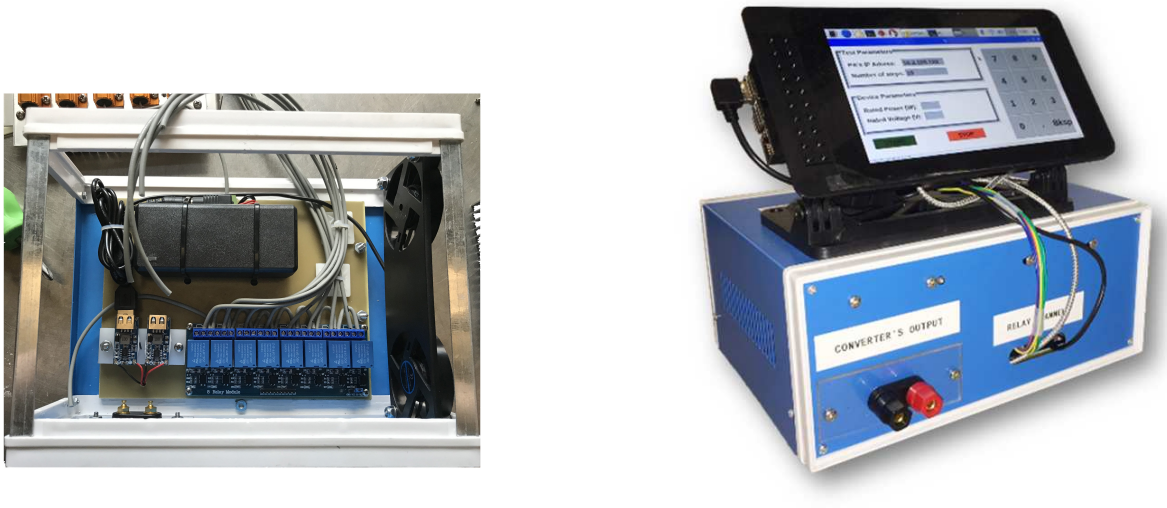


**(a)** Manufacturing Process of the CLB

**(b)** CLB built

**Figure 2.6:** Building the load bank controlled by a Raspberry Pi. (a) Preparing to wire relay channels to resistors. (b) CLB built and ready to operate.

ample, to test a converter at 10 load levels, the code calculates 10 appropriate resistance values to exercise the converter's full power range, and the combinations of resistors to achieve these values. The CLB then communicates with the power analyzer (the Keysight Power Analyzer PA2203A (PA) is described in detail in the next section) using the Standard Commands for Programmable Instruments (SCPI) interface, causing the analyzer to start the data collection.

The CLB then cycles through the load combinations three times, performing three rounds of tests at the same 10 load levels. The three replicates execute power levels in varied order to identify any converter behaviors that occurred only when moving through power steps in one order (e.g. from high-to-low, or low-to-high power):

1. Vary power monotonically increasing from minimum to rated power.
2. Vary power monotonically decreasing from rated to minimum power.
3. Vary power randomly, within the range of rated and minimum power, exercising all 10 power levels.

For every load step a .csv file is saved in a flash drive connected to the PA, containing voltage and current waveforms. This data is further processed by another python script, which extracts the harmonics magnitude and angle, as well as other electric variables like power factor, active power, etc. After the tests are performed, another python script builds three efficiency curves for the device: one for each set of test. The purpose of doing it three times is to compare the consistency of the efficiency curves obtained.

Once the first model was built and tested, two more units were replicated using the same specifications. Finally, efficiency was calculated by using the input and output power, measured by appropriate instrumentation. Running tests in this automated manner saved time, guaranteed consistency, and reduced the possibility of errors or bias. More than 30 converters have been tested, to date, in the project.

## 2.3 Measurement Equipment

As described in the previous section, measurements were made with a Keysight PA2203A power analyzer (PA) to calculate efficiency of the power converters. The PA has 4 channels, each with current (up to 50A) and voltage (up to 1000V) measurements. This device also captures and displays waveforms, and can be used to measure both AC and DC signal strength, power consumption, power efficiency and can perform harmonic analysis. The power measurement accuracy of the analyzer is 0.1%. Since the power analyzer has 4 channels, it can be used to analyze two power converters at the same time.

Depending on the tests, additional equipment was used to collect data, as follows: one Keysight 34980A multi-function measuring unit (MU) paired with a Keysight 34921T analog multiplexer; two Keysight 34461A digital multimeters; three Agilent N7973A power supplies.

The MU and multiplexer supports 40 channels AC/DC voltage, frequency, temperature or resistance, and 4 channels for AC/DC current measurements, limited to 1A. The

multimeters can handle current up to 10A. Both devices have 6 ½ digits (22 bits) of resolution.

Data was collected with a laptop through an Ethernet connection. The diagram in Figure 2.7 illustrates a setup to collect data of one AC/DC converter and one DC/DC using the PA and the CLBs.

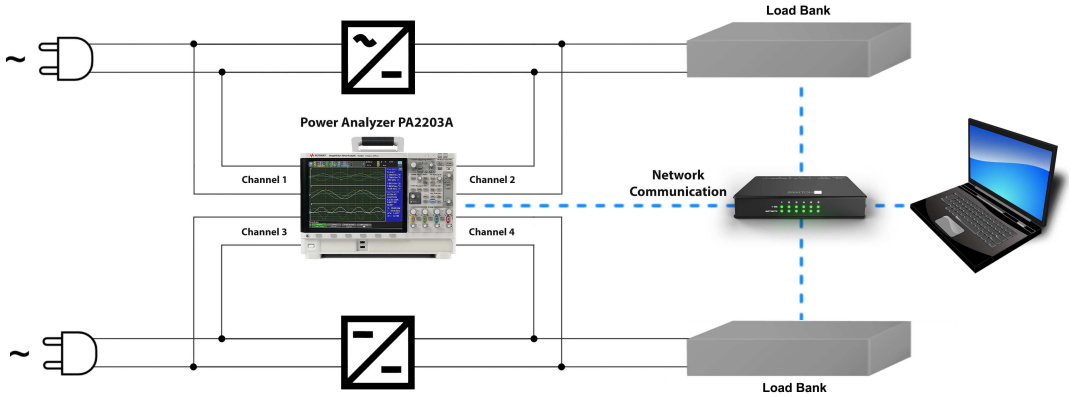


**Figure 2.7:** Testing power converters with simulated loads.

## 2.4 Methods

This section describes how the tests were performed so they provided enough data to analyze each harmonic component of each tested appliance and converter. It will also discuss how harmonics play a fundamental role in building a converter efficiency curve, and how the sample rate is important to achieve a satisfactory result. Finally, the data obtained for the appliances and converters tested will be presented.

All converters presented high harmonics, including higher frequency, high-order, harmonics. Methods in this study limited analysis to the first 128 harmonics, or 7680Hz. For these high frequency components to be analyzed according to Nyquist's theorem, the sampling frequency needed to be at least twice as large as the frequency of the signal being reproduced. This gave a minimum data collection frequency of 15360Hz.

In view of the above considerations, for each device under test, current and voltage waveforms were collected for a period of 1 second, at a collection frequency of 15.36kHz. Then, using a Fast Fourier Transform (FFT) algorithm, these waveforms were decomposed into harmonic components, with their respective magnitude and angle. The Fourier transform allows us to decompose a periodic signal into a series of signals, which include its DC component, the fundamental frequency (which in our case is 60 Hz), the second order component (120Hz), the third (180Hz) and so on. The sum of all of these components represents the collected signal.

### 2.4.1 Power Calculation in Harmonics

A periodic signal can be decomposed into a Fourier series, composed of the DC component, fundamental frequency and its harmonic components. Therefore, a voltage signal defined as $v(t) = sin(t)$ can be decomposed into:

$$v(t) = V_{DC} + \sum_{k=1}^{\infty} V_k sin(k\omega t + \theta_K) \tag{2.1}$$

In Equation 2.1, $V_k$ is the voltage magnitude, $\omega$ is the fundamental frequency in radians per second, $k$ the harmonic order, and $\theta$ is the harmonic component angle.

To calculate the real power of a distorted wave form, we need to find it for every harmonic component, and then each component's power term should be added to find the total power, as shown in equation 2.2 [50].

$$P = V_{DC} \cdot I_{DC} + \sum_{k=1}^{\infty} V_{k,rms} \cdot I_{k,rms} \cdot cos(\theta_k) = P_{DC} + P_1 + P_2 + P_3 + ... \tag{2.2}$$

The power consumed by the DC component of the signal must also be taken into account. If the component $P_{DC}$ is zero, it means the signal mean is zero and there is no DC component in it. The same equations are valid for both voltage and current; the primary emphasis in this study are current harmonics.

The fundamental harmonic power term $P_1$ is responsible for the largest contribution to the total power, and the other components are relatively small compared to the total amount, caused by current distortion due to the nonlinearity of electronic power loads. However, it is very important that smaller components are included in the power calculation as they have substantial impact on efficiency calculations, shown in Equation 2.5 in the next section.

### 2.4.2 Total Harmonic Distortion (THD)

THD is the most common measure for harmonic distortion. In general the more harmonics a signal has, the higher the THD. It can be measured for either a current or voltage signal and it disregards the DC component. The current THD is calculated as the ratio of the root mean square (RMS) of all current components (from the 2nd on) over the RMS of the fundamental (see equation 2.3).

$$THD_I = \frac{\sqrt{\sum_{k=2}^{\infty} I_{k,rms}^2}}{I_{1,rms}} \tag{2.3}$$

The same logic is applied for the voltage THD:

$$THD_V = \frac{\sqrt{\sum_{k=2}^{\infty} V_{k,rms}^2}}{V_{1,rms}} \tag{2.4}$$

## 2.5 Converters Tests

Data from this study is publically available on CSU's *Mountain Scholar* open access repository at

https://hdl.handle.net/10217/207807

or the digital object identifier:

http://dx.doi.org/10.25675/10217/207807

In the following subsection, an example will be presented which shows the step by step of how the data was analyzed individually for each converter.

### 2.5.1 Converter Test Analysis - Example

Figure 2.8 shows the voltage and current AC input waveforms (captured as depicted in figure 2.7) for an AC/DC HP laptop power supply (model PPP009L-E, input voltage 100-240VAC, output voltage 19.5VDC, 65W) at 20% load.


**(a)** HP Laptop Power Supply.

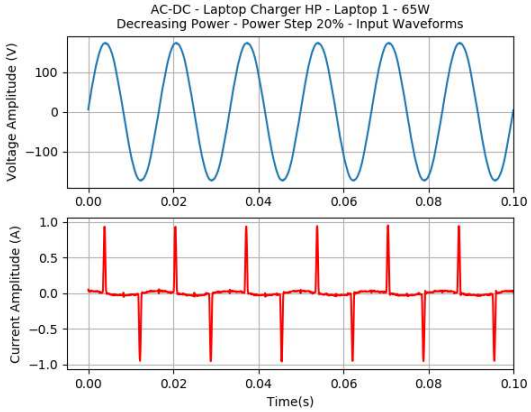


**(b)** HP Laptop Power Supply - AC Input Current and Voltage waveforms.

**Figure 2.8:** HP Laptop Charger Input Waveforms. (a) Converter specifications. (b) AC input voltage and current waveforms.

Reviewing Figure 2.9, the voltage signal is a clean sinusoidal waveform while the current is highly distorted, with sharp and equally spaced spikes of approximately with a peak magnitude of 1A. After applying the FFT to these signals, the magnitude and angles for the voltage and current input signals were extracted up to 7.68kHz.

The harmonics that are odd multiples of the fundamental frequency are called odd harmonics (3f, 5f, 7f, 9f ...), and those that are even multiples are even harmonics (2f, 4f, 6f, 8f ...).

With the converter being loaded at only 20%, the current magnitude is low and not able to produce a significant voltage distortion, and therefore we can see that the fundamental accounts for virtually the entire voltage signal. On the other hand, we can see a

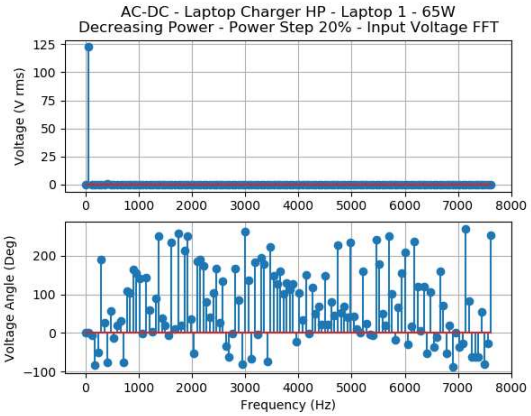


**(a)** HP Laptop Power Supply - Input Voltage FFT.

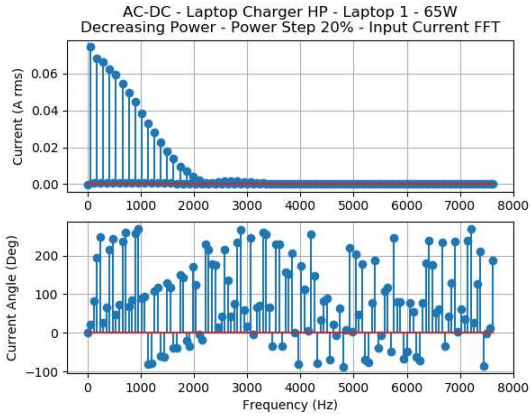


**(b)** HP Laptop Power Supply - Input Current FFT.

**Figure 2.9:** HP Laptop Charger Input Waveforms FFT. (a) AC Input Voltage FFT. (b) AC input current FFT.

significant number of current harmonic components below 2kHz and some small contributions up to 3.5kHz. Overall, they are mainly odd components.

In power systems, even harmonics are normally negligible when compared to odd components, since most even harmonic waveforms have half-wave symmetry. In other words, if the positive and negative halves of a waveform are symmetric, the signal primarily contains fundamental and odd components.

Figure 2.10 depicts the converter's DC output current and voltage, and their respective means.

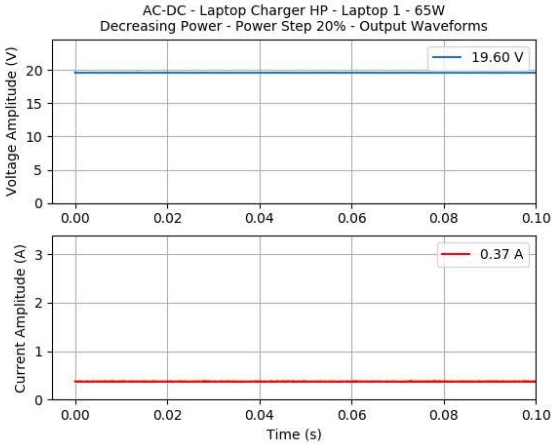


**Figure 2.10:** HP Laptop Power Supply - DC Output Current and Voltage waveforms.

Figure 2.11 confirms, using FTT, the presence of the DC component without any harmonics, as it is constant over time.

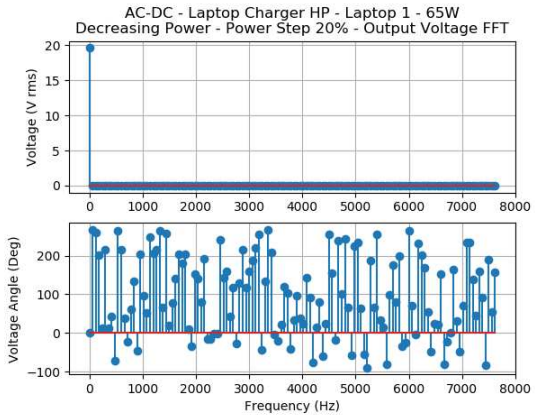


**(a)** HP Laptop Power Supply - Output Voltage FFT.

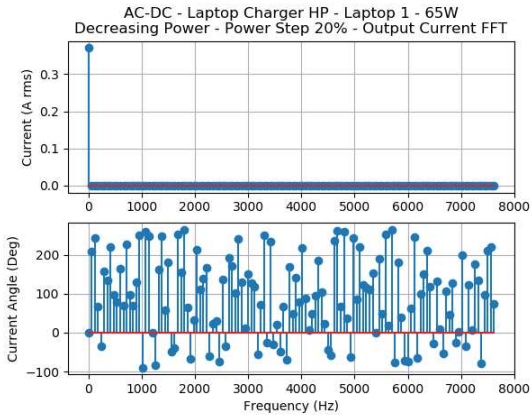


**(b)** HP Laptop Power Supply - Output Current FFT.

**Figure 2.11:** HP Laptop Charger Output Waveforms FFT. (a) DC Input Voltage FFT. (b) DC input current FFT.

With all this information, it is now possible to calculate the real input AC power (equation 2.2), the output DC power, the $THD_I$ and $THD_V$ for the AC waveforms (eq. 2.3 and 2.4, respectively), and the converter efficiency at this load level (eq. 2.5).

$$Eff(\%) = \frac{Output\ Power}{Input\ Active\ Power} \cdot 100 \tag{2.5}$$

Table 2.1 shows the results for these calculations.

**Table 2.1:** Calculations for the HP laptop converter

| Electric Variable | Result |
|---|---|
| Input Voltage RMS (V) | 122 |
| Input Current RMS (A) | 0.19 |
| Input Active Power (W) | 8.47 |
| Input THDV (%) | 0.54 |
| Input THDI (%) | 226 |
| Output Voltage RMS (V) | 19.6 |
| Output Current RMS (A) | 0.37 |
| Output Power (W) | 7.27 |
| Efficiency (%) | 85.9 |

The above calculations for this given converter describe one load step, at 20% of its rated power. To build the converter's efficiency curve, the same calculations were performed for the remaining load levels, from 0% to 100%. As described in Section 2.2, a CLB was used to load the converter and three sets of tests were performed by the CLB: increasing the power, decreasing it, and cycling through random power steps. After collecting the data for all load levels, the efficiency curves were built (Fig. 2.12).

For this converter, the three efficiency curves are similar, which indicates that the order in which the load steps are applied to the converter do not impact calculation of the converter's efficiency.

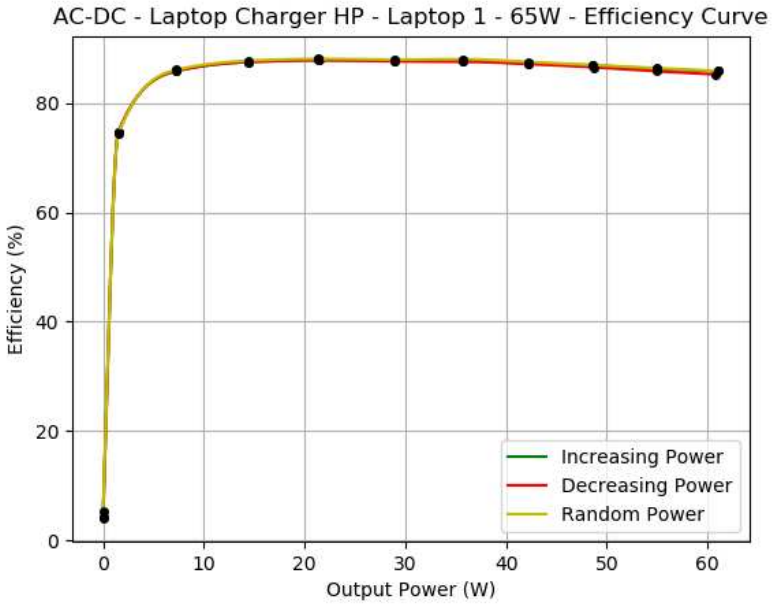


**Figure 2.12:** HP Laptop Power Supply - Efficiency Curve.

## 2.6 Appliances Tests

In addition to the converters, other appliances with internal converters were also measured, including televisions, screens, coffee makers, refrigerators, projectors, fans, soldering stations, etc. As there is rarely external access to the AC/DC converters in these appliances, power consumption and harmonic data were collected from the AC supply to the appliances, while forcing each into different operating modes. A TV was analyzed, for example, when in standby, when the screen was totally black, totally white, and playing a video. The link below contains the full data set.

https://hdl.handle.net/10217/207807

# Chapter 3

# Appliances Power Consumption

The characterization described in the previous chapter provides data about the efficiency and harmonic content of converters. This chapter augments this data with power consumption profiles for the converters in normal use. Usage measurements were made on a group of appliances in use at the Powerhouse Energy Campus at CSU, over a period of approximately 2 months. The appliances studied in this chapter were divided into five groups: laptops, desktops, screens, printers and network devices.

The data collection was performed with smart plugs connected to a private network. However, it was later discovered these smart plugs have a substantial time constant when reading time-varying power consumption, which must be corrected during data analysis. After processing the collected signals, the power level distribution for the AC/DC converters of each appliance was analyzed.

## 3.1 Methods

Although MEL converters usually indicate their rated power on nameplates, the weighted power consumption over time is often lower during actual operation – i.e. the converter rating exceeds that of the load. Each power consumption level experienced during device operation has an associated conversion efficiency value. An AC/DC laptop converter that reaches a peak efficiency of 93%, for example, says little about the device's net efficiency if the equipment operates at a lower level most of the time. Therefore the rated power is not very representative of actual energy consumption by a device. Hence, if a device's actual power consumption is collected over a given period of time, it's power level distribution may be compared to the rated power for each device.

In this study, power consumption data from 27 AC appliances was collected using WEMO smart plugs for an approximately two months. The following sections will cover

how the smart plug time constant was identified and mitigated, what was done to process the data, details about the appliances analyzed, and the results gathered.

### 3.1.1 Run Time Measurements

#### Evaluating the Smart Plug Accuracy

The WEMO smart plugs used in this experiment are all model F7C029V2, rated for 120VAC and 15A. Before analyzing the data collected, it was essential to test the accuracy of these devices. This was done using a load bank to load one smart plug at different low power levels. Low power levels theoretically produce the largest relative measurement errors, as accuracy was quoted for the maximum measurement of the device. Table 1 shows the resistor values and the respective power draw for each at 120VAC.

**Table 3.1:** WEMO Low Power Test - Resistors used

| Low Power Resistors | |
|---|---|
| Resistance (kΩ) | Power at 120VAC (W) |
| 143 | 0.10 |
| 47 | 0.31 |
| 30 | 0.48 |
| 20 | 0.72 |
| 15 | 0.96 |
| 10 | 1.44 |
| 7.5 | 1.92 |
| 6 | 2.40 |
| 5 | 2.88 |
| 3.5 | 4.11 |

A private network was set up and connected to the WEMO, the Power Analyzer (PA), and one laptop to gather the data. A ten-position switch was used to vary the resistors connected to the smart plug every 2 minutes, while data was collected from two sources simultaneously: the WEMO, via wi-fi and read through a python script at 1Hz, and the

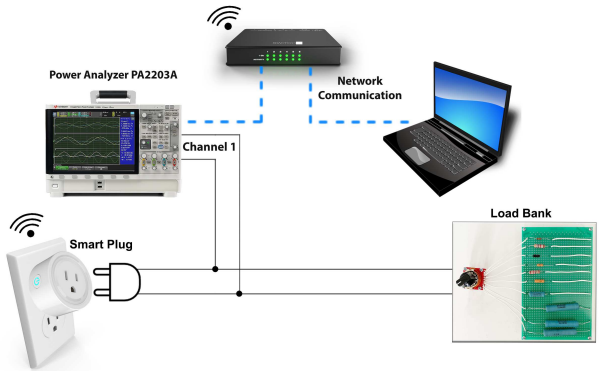


**Figure 3.1:** Setup configuration for smart plug accuracy test.

high precision PA2203A. Figure 3.1 shows the test setup and Figure 3.2 plots the data collected.

In these data plots, we can observe the power steps performed and the measurement errors of the WEMO relative to the reference instrument (the power analyzer). Most notably, there is a time delay on the measurements reported by the WEMO at the moment of the load change. This is the largest source of error for the WEMO measurements. Excluding period with a visible time constant effect, the average error of the WEMO over the the entire experiment was 0.05W. While the time delay could be easily removed in this experiment with measurements made at stable conditions for two minutes, the time constant causes larger errors when the power level changes quickly or frequently, as discussed in the next subsection.

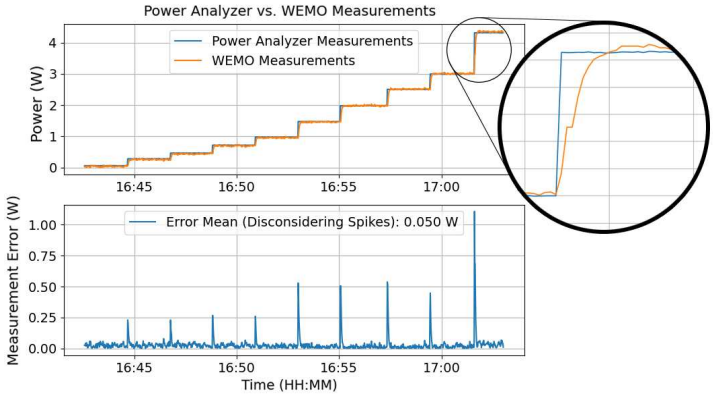


**Figure 3.2:** WEMO power measurements.

### WEMO Time Constant

In order to characterize the observed WEMO time constant ($\tau$), two other tests were performed with purely resistive loads that draw the following amounts of power at 120VAC: 30W, 77.7W, 108.4W, 152.5W, 179.9W, 183.2W, 224.7W, 300.4W, and 330.5 W. The WEMO was connected to each load one at a time, starting from no load up to the largest power draw. These load steps were saved in a .csv file. Then, the test was repeated in the opposite direction, starting at the highest load and ended at no load.

The power steps were then normalized and, given their apparent exponential rise/decay, the curves were fit to a first order transfer function: $\frac{1}{\tau * s + 1}$. From there, the mean for the time constant $\tau$ was calculated (Fig. 3.3).

The average values for the decaying and rising curves were similar (2.75s and 2.79s respectively). Taking the average of those two values, an overall mean for $\tau$ was calculated at 2.77 seconds.

### Recovering the True Power Signal

Due to the time constant of the WEMO power measurement, power measurements reported by the smart plug have errors when the true power consumption of the appliance varies rapidly. In addition, there is random noise in the WEMO measurements. To better

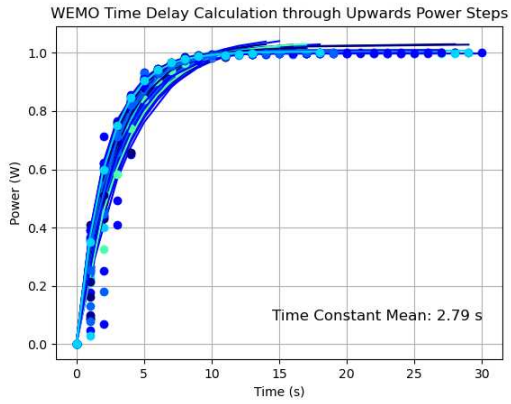


**(a)** WEMO Upwards Power Steps.

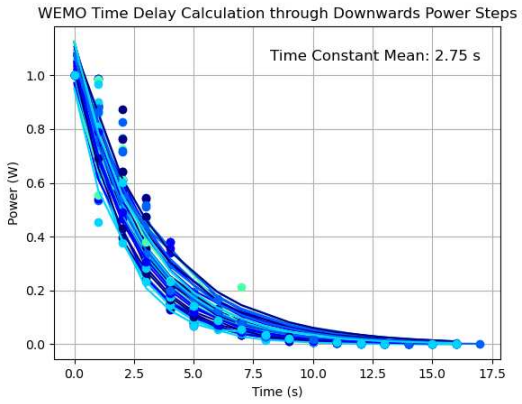


**(b)** WEMO Downwards Power Steps.

**Figure 3.3:** WEMO Time Constant Calculation. (a) WEMO Upwards Power Steps. (b) WEMO Downwards Power Steps.

estimate actual power consumption, the data reported by the WEMOs must be processed in order to calculate the true power level distribution values of the appliances.

An inverse transfer function would be appropriated for the elimination of the time delay, however the exact inverse function ($\tau * s + 1$) requires differentiation and is therefore improper. Instead, we ran the WEMO signal through an approximate inverse transfer function, shown in eq. 3.1. As long as $T$ is much smaller than $\tau$, this transfer function is implementable. Hence, T is tuned at 0.1, and the resultant signal is then connected to a low pass filter to reduce noise. This provides an estimate of the true power signal consumed by each device, called "recovered power signal" from this point forward. The next section describes its error.

$$\frac{\tau * s + 1}{T * s + 1} \tag{3.1}$$

**Recovered Power Signal Error**

The worst case scenario, with the greatest estimated noise and large variations in the true power signal, was evaluated through a simulation developed in Simulink/MATLAB

(Fig. 3.4). Using it, the maximum error associated with recovered power signal was calculated.

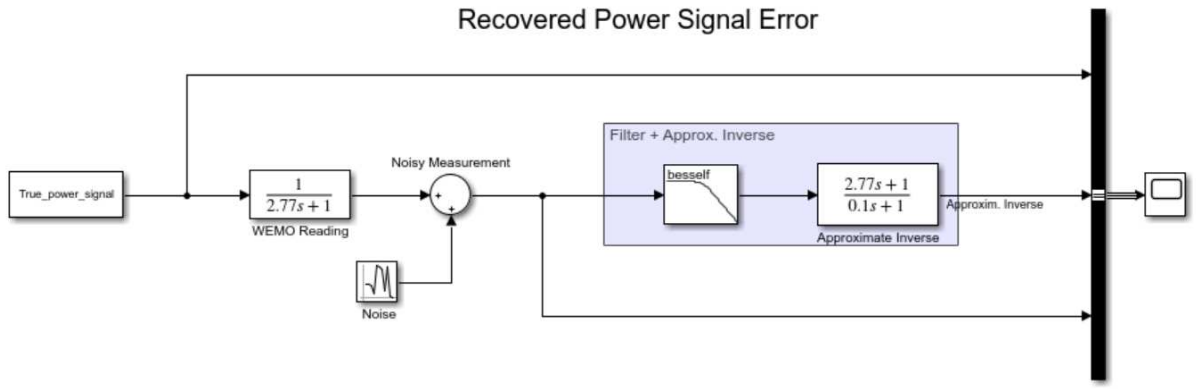


**Figure 3.4:** Simulation to calculate the error in the recovered power signal.

A random signal was created, represented by the block *True power signal*, varying from 0W to 100W in steps of 10%, with duration between 1 and 4 seconds, with 0.1 second of resolution. Then, to simulate the WEMO, it was passed through a first order transfer function containing the calculated WEMO time constant, and noise was added.

The worst case scenario noise was calculated using the relative variance of the 1 Hz WEMO signal when the WEMO was measuring a low load of 4.5W. The same relative noise was applied to all loads, up to a maximum of 100W – a conservative estimate of noise level. Finally, the resultant signal was sent through a Bessel filter (8th order, pass-band edge frequency of 1Hz) and the approximate inverse transfer function, as described above. Figure 3.5 shows the true power signal, the recovered power signal, and the signal reported by the WEMO for 60 seconds of simulation.

It is possible to recover a reasonably accurate approximation of the true power signal. However, before being able to calculate the exact approximation error, it is necessary to eliminate the phase shift between the two signals, caused by the low pass filter.

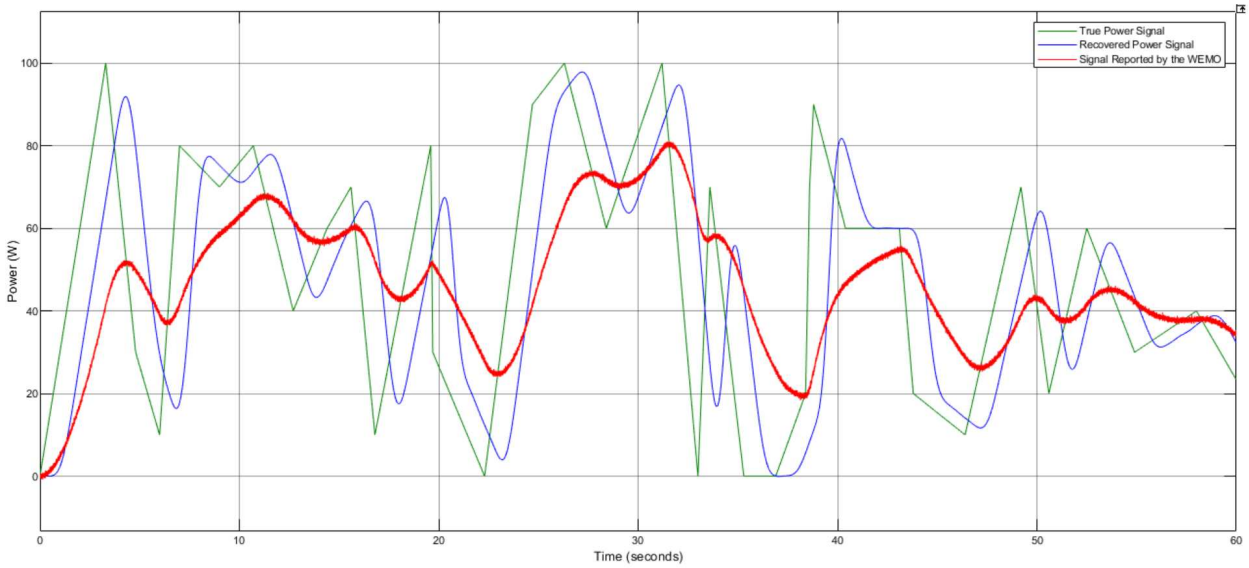


**Figure 3.5:** Recovered power signal - Simulation results.

A Bessel filter was used because it is a linear phase filter, which means it has a consistent delay at every frequency. This allows us to simply shift back the recovered power signal by 1073ms (delay found), using a post-processing script in python, to match the true power signal and calculate the absolute difference between them.

Figure 3.6 depicts the true and recovered signals overlapped, along with the absolute error, for a 600 second simulation.

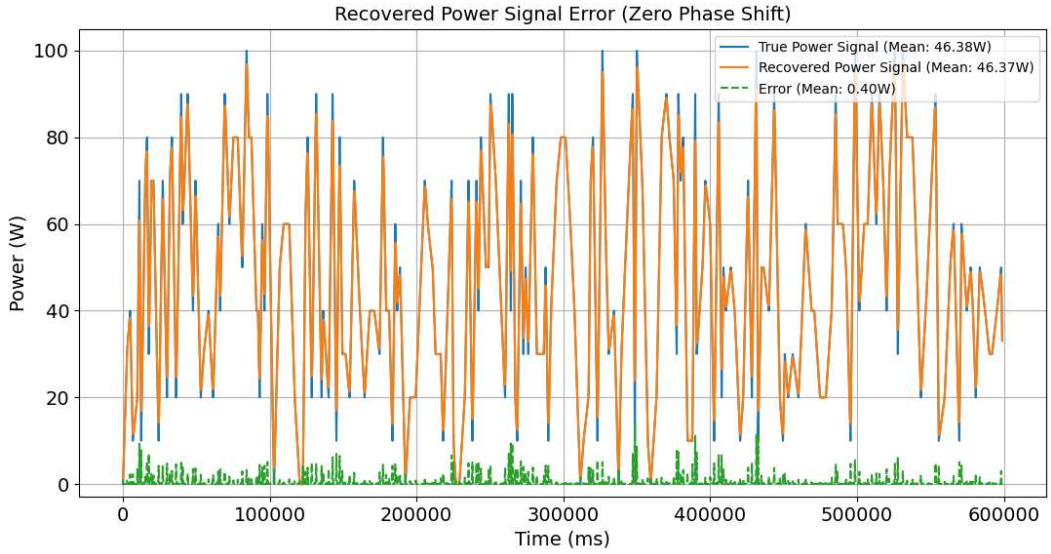


**Figure 3.6:** Recovered power signal - Error.

Dividing the sum of the absolute error by the sum of the recovered signal produces an error of 0.87%, illustrating that the signal processing was able to perform recover the original power signal to within 1% accuracy. Errors are largest where the rate-of-change of the power signal is highest. That error is due to the low pass filter, which attenuates the high frequencies present in these fast-changing values, but is necessary to eliminate noise prior to the time constant recovery.

### 3.1.2 Appliances Analyzed

In this work, power consumption data from 27 devices were collected with 27 WEMOs, during an period of two months, at a frequency of 1Hz. The appliances analyzed here are commonly found in an office environment, and were divided in five groups: laptops, screens, work stations, printers, and network appliances. Table 3.2 shows their models and converters.

For the external converters, the rated power information was extracted directly from their name plates. For the internal converters, it was extracted from online sources [51–55].

**Table 3.2:** Appliances Monitored

| Smart Plug | Appliance | Converter Specification | Output Power (W) |
|---|---|---|---|
| WEMO 1 | HP Laptop | AC/DC - External - Model 854056-002 | 90 |
| WEMO 2 | DELL Laptop Inspiron | AC/DC - External - Model LA45NM140 | 45 |
| WEMO 3 | HP Laptop | AC/DC - External - Model TPN-CA04 | 45 |
| WEMO 4 | Microsoft Laptop | AC/DC - External - Model 1620 | 48 |
| WEMO 5 | Microsoft Laptop | AC/DC - External - Model 1749 | 90 |
| WEMO 6 | Microsoft Laptop | AC/DC - External - Model 1749 | 90 |
| WEMO 7 | HP Laptop | AC/DC - External - Model GB4943 1-2011 | 65 |
| WEMO 8 | Microsoft Laptop | AC/DC - External - Model 1749 | 90 |
| WEMO 9 | ViewSonic Screen | AC/DC - External - Model VX2703MH-LED | 36 |
| WEMO 10 | HP Screen EliteDisplay E232 | AC/DC - Internal | 35 |
| WEMO 11 | HP Screen EliteDisplay E232 | AC/DC - Internal | 35 |
| WEMO 12 | HP Screen EliteDisplay E232 | AC/DC - Internal | 35 |
| WEMO 13 | HP Screen EliteDisplay E242 | AC/DC - Internal | 38 |
| WEMO 14 | ACER Screen CB241HYK | AC/DC - Internal | 60 |
| WEMO 15 | DELL Screen P2415Qp | AC/DC - Internal | 90 |
| WEMO 16 | HP Screen EliteDisplay E232 | AC/DC - Internal | 35 |
| WEMO 17 | HP Screen EliteDisplay E273 | AC/DC - Internal | 42 |
| WEMO 18 | HP Screen EliteDisplay E273 | AC/DC - Internal | 42 |
| WEMO 19 | Apple Thunderbolt Display | AC/DC - Internal | 250 |
| WEMO 20 | DELL Screen E2010Ht | AC/DC - Internal | 26 |
| WEMO 21 | Phillips 4k Screen 288P6L | AC/DC - Internal | 60 |
| WEMO 22 | HP Z240 Tower Workstation | AC/DC - Internal | 400 |
| WEMO 23 | HP Z240 Tower Workstation | AC/DC - Internal | 400 |
| WEMO 24 | HP Printer LaserJet 1022 | AC/DC - Internal | 300 |
| WEMO 25 | HP Printer OfficeJet Pro 9018 | AC/DC - Internal | 30 |
| WEMO 26 | Netgear ReadyNAS RN31600 | AC/DC - Internal | 200 |
| WEMO 27 | Netgear WNR2000 v3 | AC/DC - External - Model LSE0107A1236 | 36 |

## 3.2 Appliances' Converters Usage

Based on the data collected from each appliance by the smart plugs and their nominal power, their operational power range was analyzed on a daily basis. Each group of appliances are represented by the following WEMOs:

- Laptops: WEMO 01 - WEMO 08
- Screens: WEMO 09 - WEMO 21
- Desktops: WEMO 22, WEMO 23
- Printers: WEMO 24, WEMO 25
- Network Appliances: WEMO 26, WEMO 27

When the devices power consumption was lower than 1W, it was considered off. Data for each appliance is represented by a box-plot, which shows the distribution of their respective power consumption. The box-plots were built based on a 95% confidence interval, and the outliers are values outside this range. It is explained in detail in figure 3.7. Figure 3.8 shows the results for all 27 appliances analyzed during the time they were on.

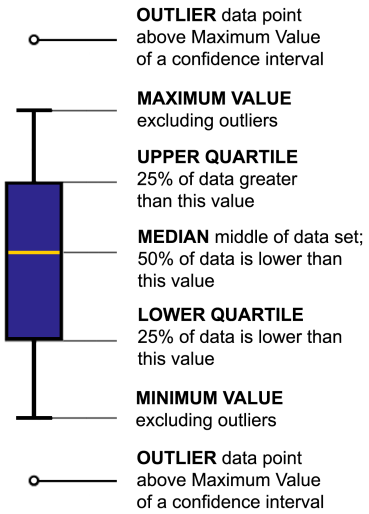


**Figure 3.7:** Box-plot interpretation

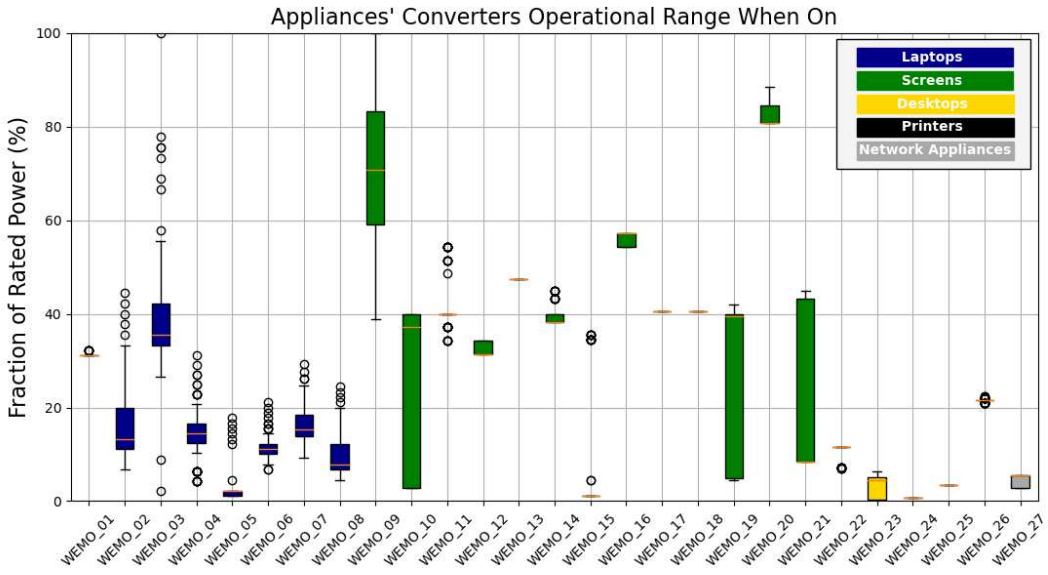


**Figure 3.8:** Appliances' converters operational range when on

Tables 3.3, 3.4, 3.5, 3.6, and 3.7 show data for converters of laptops, screens, desktops, printers, and network appliances groups, respectively. The tables provide data for each converter concerning the percentage of the time the device was off during the data collection, rated power, the maximum fraction of rated power (MFRP) in a 95% confidence interval and the typical load. The typical load is defined by the interquartile range (IQR) from the 25th to the 75th percentile.

In the laptops group, the overall typical load is between 10-42% of the converters rated power. The MFRP is 55.6%, and 7 of 8 laptop converters were never loaded with more than 34% of their capacity. In other words, for 87.5% of the cases, converters were over-sized in at least 2.95 times. The converter connected to WEMO 05 has an atypical load range of only 1.1-2.2%, because when the laptop was on, it was often in sleep mode.

In regards to the screens only 1 was on 60% of the time, while all the others were on for only 0.8%-17.1%. WEMOs 09 and 21 have the highest MFRP of 88.5% and 100%, respectively, while 60% of the screens have their MFRP equal or below 42%, indicating that they are also over-sized for their respective loads. Excluding WEMOs 09 and 21, the

**Table 3.3:** Laptops Analysis

| | Time off (%) | Rated Power (W) | Typical Load (%) | MFRP (%) |
|---|---|---|---|---|
| WEMO 01 | 93.0 | 90.0 | 31.1 - 31.1 | 31.1 |
| WEMO 02 | 93.7 | 45.0 | 11.1 - 20.0 | 33.3 |
| WEMO 03 | 86.1 | 45.0 | 33.3 - 42.2 | 55.6 |
| WEMO 04 | 1.0 | 48.0 | 12.5 - 16.7 | 20.8 |
| WEMO 05 | 43.9 | 90.0 | 1.1 - 2.2 | 2.2 |
| WEMO 06 | 86.9 | 90.0 | 10.0 - 12.2 | 14.4 |
| WEMO 07 | 81.8 | 65.0 | 13.8 - 18.5 | 24.6 |
| WEMO 08 | 0.0 | 90.0 | 6.7 - 12.2 | 20.0 |

**Table 3.4:** Screens Analysis

| | Time off (%) | Rated Power (W) | Typical Load (%) | MFRP (%) |
|---|---|---|---|---|
| WEMO 09 | 91.3 | 36.0 | 59.0 - 83.3 | 100 |
| WEMO 10 | 84.2 | 35.0 | 2.9 - 40.0 | 40 |
| WEMO 11 | 91.7 | 35.0 | 40.0 - 40.0 | 40 |
| WEMO 12 | 99.2 | 35.0 | 31.4 - 34.3 | 34.3 |
| WEMO 13 | 94.1 | 38.0 | 47.4 - 47.4 | 47.4 |
| WEMO 14 | 90.1 | 60.0 | 38.3 - 40.0 | 40 |
| WEMO 15 | 39.3 | 90.0 | 1.1 - 1.1 | 1.1 |
| WEMO 16 | 87.7 | 35.0 | 54.3 - 57.1 | 57.1 |
| WEMO 17 | 87.8 | 42.0 | 40.5 - 40.5 | 40.5 |
| WEMO 18 | 87.8 | 42.0 | 40.5 - 40.5 | 40.5 |
| WEMO 19 | 82.9 | 250.0 | 4.8 - 40.0 | 42 |
| WEMO 20 | 84.1 | 26.0 | 80.8 - 84.6 | 88.5 |
| WEMO 21 | 84.1 | 60.0 | 8.3 - 43.3 | 45 |

typical load is in the range of 2.9-57.1%. The low limit of the typical load might be because the device entered in stand-by mode.

The two desktops analyzed belong to graduate students that work part time at the laboratory. They are both rated at 400W, and their MFRP are 6.3% and 11.5%. These devices are on at least 98.5 % of the time, and although they are constantly used to perform heavy simulations in the laboratory, the typical load showed in 3.5 shows that the converters are underloaded, and could use up to 8.7 times the maximum power they are drawing. Part of this is explained by the fact that some available resources are not often used, such as USB ports and sound system, for example.

**Table 3.5:** Desktops Analysis

| | Time off (%) | Rated Power (W) | Typical Load (%) | MFRP (%) |
|---|---|---|---|---|
| WEMO 22 | 0 | 400.0 | 11.5 - 11.5 | 11.5 |
| WEMO 23 | 1.5 | 400.0 | 0.2 - 5.0 | 6.3 |

Two printers were also analyzed and their analysis is showed in table 3.6. One has a typical load of only 0.7% of its rated power (300W), and the other 3.3% of 30W. These values match with their MFRP. One printer is used by one staff only, and the other is a family printer. One stays on 89% of the time, and the other 99%, and because they are rarely in print work, the power consumption when they were printing (above the typical load) were considered as outliers. However 23W was the maximum power achieved by printer connected to WEMO 25 for 0.01% of the time and 5W was the maximum power recorded for WEMO 24 for 1.12e-06% of the time.

**Table 3.6:** Printers Analysis

| | Time off (%) | Rated Power (W) | Typical Load (%) | MFRP (%) |
|---|---|---|---|---|
| WEMO 24 | 10.6 | 300.0 | 0.7 - 0.7 | 0.7 |
| WEMO 25 | 0.3 | 30.0 | 3.3 - 3.3 | 3.3 |

WEMO 26 and 27 are connected to the Netgear ReadyNAS RN31600 and to the router that was used to set up the private network to the 27 WEMOS. Both were on 100% of the time. While the first has an internal converter, the router is connected to an external AC/DC, which is not the original one provided by the manufactured. It is using another converter found in the lab, which has the same output voltage but is rated for 36W. Although this is way above the device actual power consumption (3.1W), we decided to keep it in this study, as this is a situation which likely could happen in the real world for different MELs. According to table 3.7, the Netgear ReadyNAS RN31600 has a MFRP of

**Table 3.7:** Network Appliances Analysis

| | Time off (%) | Rated Power (W) | Typical Load (%) | MFRP (%) |
|---|---|---|---|---|
| WEMO 26 | 0 | 200.0 | 21.5 - 21.6 | 21.6 |
| WEMO 27 | 0 | 36.0 | 2.8 - 5.6 | 5.6 |

21.6%, with the same value for its typical load, indicating the converter is almost 5 times over-sized for its maximum load recorded. For the router, as expected, the typical load range and the MFRP were very low: 2.8-5.6% and 5.6%, respectively.

An interesting point is that 88.9% of all the appliances' converters never operate above 60% of their rated capacity, and 87.5% of these have their IQR below 42%. This shows that for all groups analyzed, it was found that converters are over-sized for the maximum power recorded for the appliances. This has at least two significant implications. First, the efficiency of these converters, weighted by load, may differ substantially from the peak efficiency of the converter. And second, since harmonics vary with power level, the harmonics injected into the system will be lower than harmonics measured at near rated load.

# Chapter 4

# Harmonics in AC appliances and AC converters

One of the advantages of a DC distribution system is the potential elimination losses from harmonic currents. Harmonics in power systems are caused by non-linear loads, such as switching power supplies using semiconductor switches (e.g. MOSFETS or transistors) and diodes. Since the majority of MELs found in commercial buildigns use internal or external switching supplies to transform AC into DC, substantial higher-order current harmonics are generated on the AC circuit. These harmonics may cause substantial problems in AC power systems, including the heating of cables, triggering protection equipment, causing measurement errors, reducing distribution component lifespans, and increasing system power losses.

In this chapter, the total harmonic distortion for different load levels on the converters was investigated, along with the potential relationship between load level and the amount of harmonics injected into the system. Additionally, two simulations were performed to investigate harmonic cancellation when many converters are connected to the same system, each of them operating at different load levels.

## 4.1 Switch-mode Power Supplies

Regarding single phase power supplies, there are two ways to supply the desired power: reducing the AC input voltage to the desired output voltage for the DC bus, which can be done with a transformer followed by a rectifier and smoothing circuit; or rectifying to DC and then converting the rectified DC voltage to the desired DC output voltage using a switch-mode power supply built with lightweight electronic components (see Figure 4.1). The second option preferred because it is cheaper, lighter, more efficient, and occupies less space than the first [56].

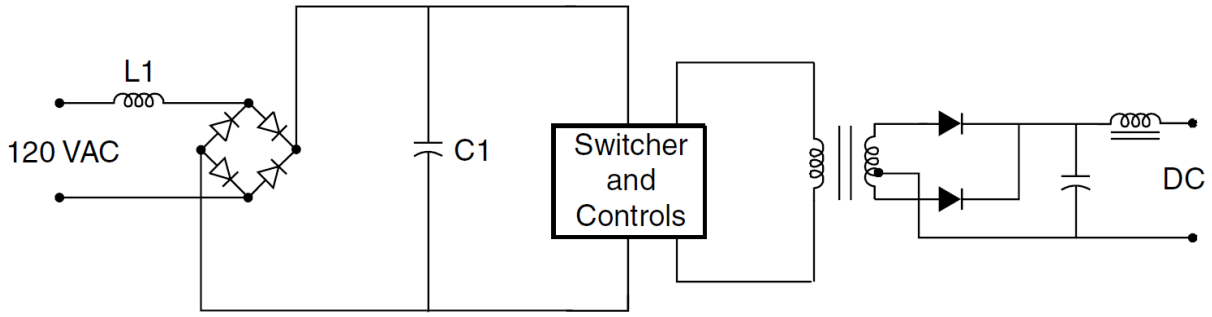


**Figure 4.1:** Full bridge switch mode power supply circuit. [56].

The figure 4.1 represents the full bridge topology, one of several types of switch-mode power supply. Different topologies are available depending on the power, reliability and efficiency desired, with a variety of circuit designs. Among these topologies, one can cite buck, boost, buck-boost, and half bridge converters. Due to its simplicity, flyback converters are also commonly used in computer screens and TVs, as it has the advantage of having fewer components [57].

In figure 4.1, the rectifier bridge converts from AC to DC, and then the switcher transforms the voltage back to AC at a high frequency so a transformer can convert it to a lower voltage, which is again rectified to DC. The transformer here is much smaller because of the high frequency of operation. As the frequency increases, the core area can be substantially reduced, reducing the copper needed and its cost. These switch-mode power supplies are typically found in laptops, phone chargers, desktops, printers and many other MELs.

A common characteristic between switch-mode power supplies, due to switching at high frequencies, is the presence of the third harmonic component. In a 3-phase 4-wire system, this third component is added to the neutral and could potentially overload it.

Generally, as the current is defined by the load, THDI tends to be high, and that tends to degrade the voltage signal. Equation 2.3 showed that a high THDI can be caused not only by high harmonic levels but also by a low fundamental value. The next section

investigates if there is any correlation between THDI and the converter output power, analyzing data from real converters collected in the lab.

## 4.2 Results

More than 30 AC/DC converters were tested at different load levels, and THDI was calculated for each load step. In order to help with the analysis, these converters were divided into the following groups: laptop chargers, phone chargers, LED drivers, chassis power supplies, workbench power supplies, fans, label printers, monitors, switches, and credit card machines. The following subsections present the results found for each group.

### 4.2.1 Laptop Chargers

The graph below shows THDI over the rated power percentage for nine converters (Fig. 4.2). With the exception of the one represented by the orange curve, the converters present very similar behavior. There is a peak THDI value of 167-238% between 0% and 30% of their rated power, indicating that the greatest generation of harmonics occurs within this range, and the distortion decreases to 120-170% at 100% rated power. The orange curve represents a 90W DELL converter, which has power factor correction in its electronic board that lowers the THDI index compared to the other devices.

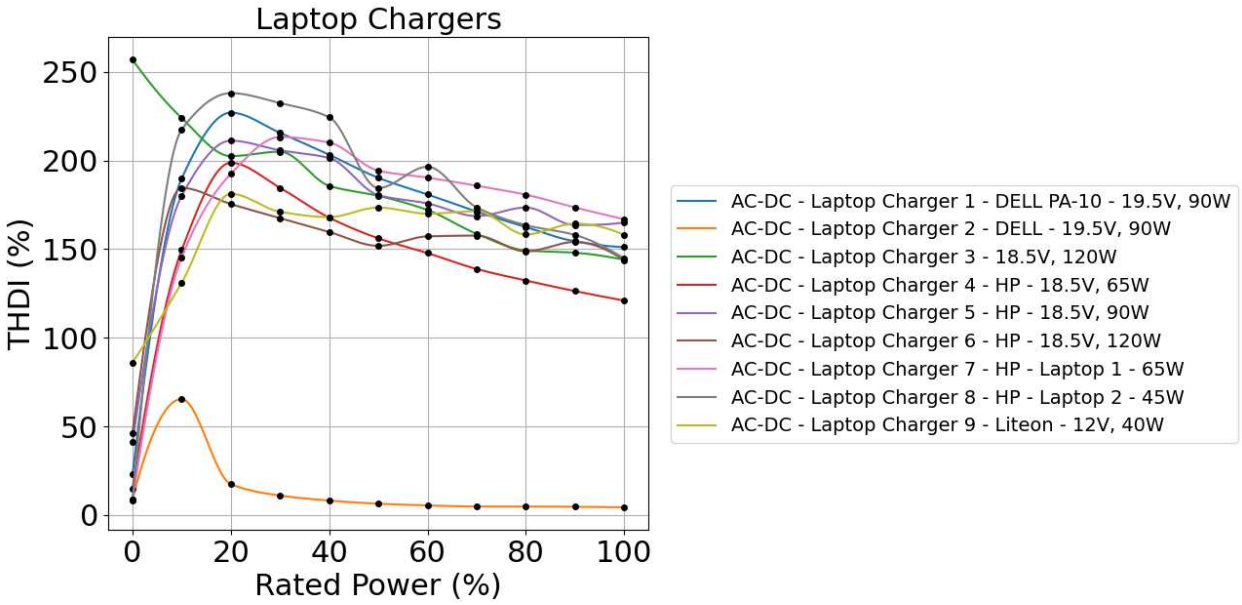


**Figure 4.2:** Laptop Chargers - THDI.

### 4.2.2 Phone Chargers

The THDI for phone chargers is higher than the laptop chargers, reaching more than 500% for the iphone charger (Fig. 4.3). However, that happens when the device is in standby mode and the output current is close to zero. More generally, the higest THDI levels for phone chargers occurs between 0% and 20% of the rated power. The phone chargers tested are all below 5 Watts and include Apple, Samsung, LG, and Nokia brands.

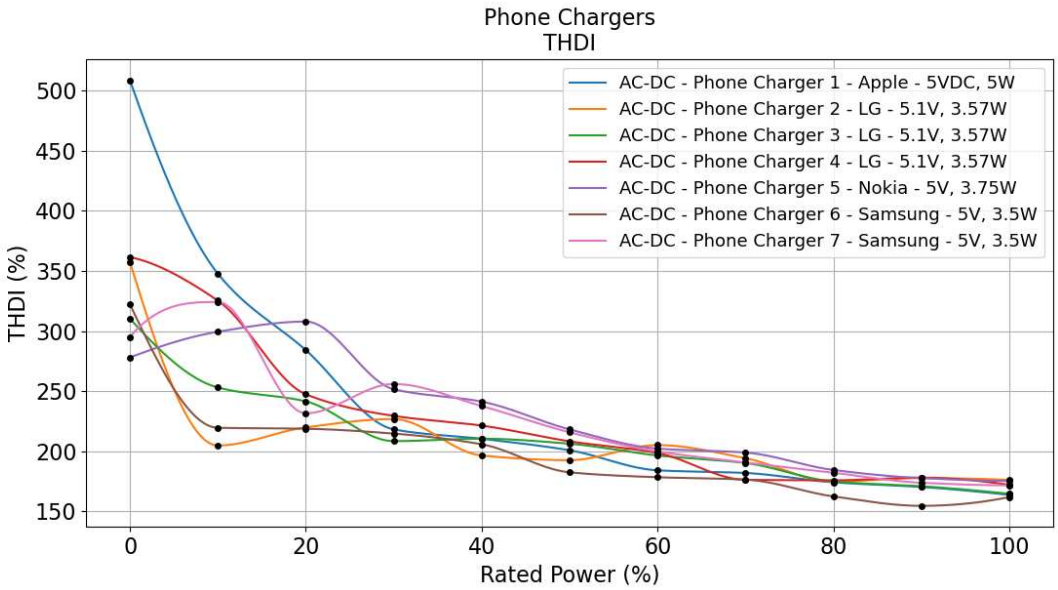


**Figure 4.3:** Phone Chargers - THDI.

### 4.2.3 LED Drivers

The three LED drivers tested are of the same model (Mean Well APV-25-24). Since their output voltage is 24V, they could not be tested with a CLB, and were loaded by combinations of resistors in parallel. As with previous converters, they present high THDI values, with the peaks close to 190% THDI at loads between 15% and 20% rated power.

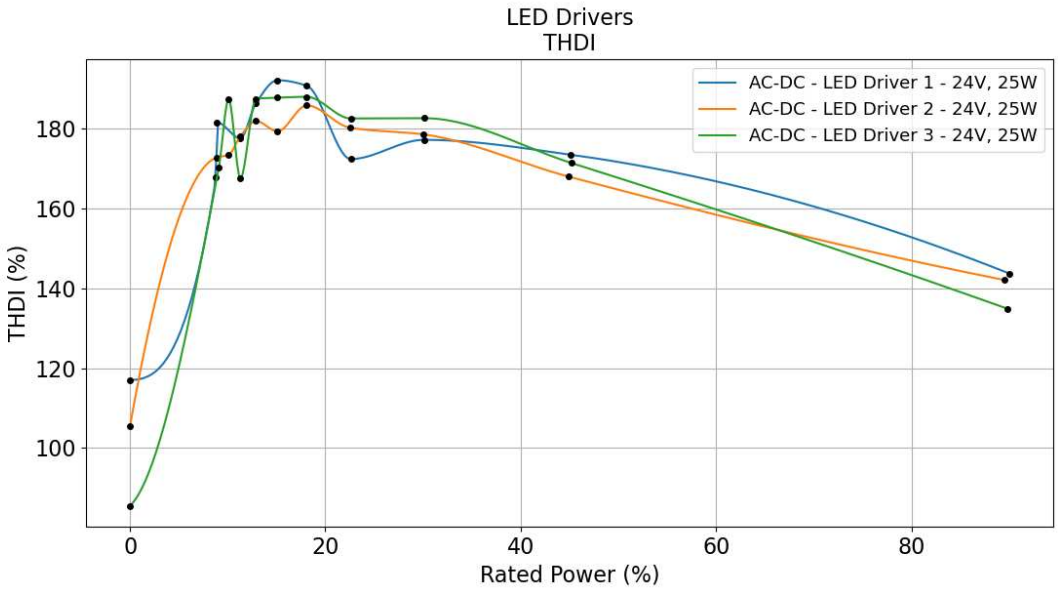


**Figure 4.4:** LED Drivers - THDI.

### 4.2.4 Chassis Power Supplies

All tested chassis power supplies have similar THDI levels despite their rated power ranging between 30W and 1000W. As seen in Figure 4.5, starting at no load, THDI rises 125% before 20% of the rated power with the peaks between 0% and 30% of rated load, with one exception. As with the laptop converters, the power supply represented by the green curve is a power supply that has a PFC, similar to the 90W DELL laptop converter mentioned earlier, which dramatically lowers its THDI values.

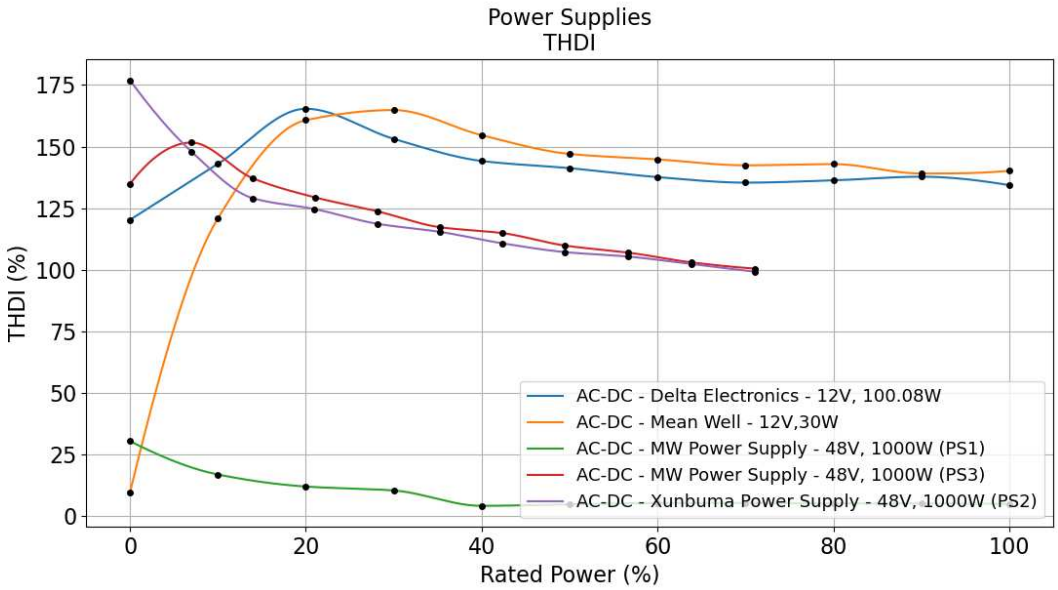


**Figure 4.5:** Chassis Power Supplies - THDI.

### 4.2.5 Workbench Power Supply

There is the same pattern in the two workbench power supplies, with THDI below 190% and peaks between 0% and 20% of the converter's rated power.

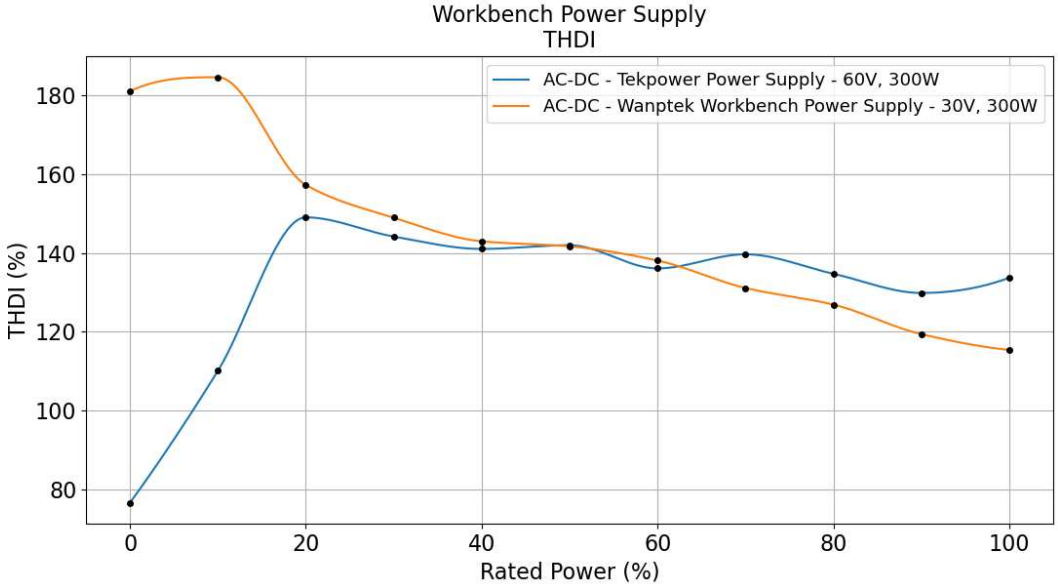


**Figure 4.6:** Workbench Power Supplies - THDI.

### 4.2.6 Switch, Label Printer, Monitor, Fan and Credit Card Machine

The converters tested in this section were:

- Netgear Switch, model SAL012F1, 12W, 100-120VAC to 12VDC
- Fan, using a switching adapter model SUN-0900070, 6.3W, 100-240VAC to 9VDC
- Brady label printer, which uses an adapter model EA1024F2-090, 27W, 100-240VAC to 9VDC
- Monitor HP Pavilion adapter 25xw, 45W, 100-240VAC to 12VDC
- Verifone Credit card machine, using an adapter model Au-79DMu, 13.5W, 100-240VAC to 6VDC

The THDI curves of these converters also followed a similar pattern, with the highest THDI values between 200% and 300%, and located between 0% and 30% of the converter's rated power.

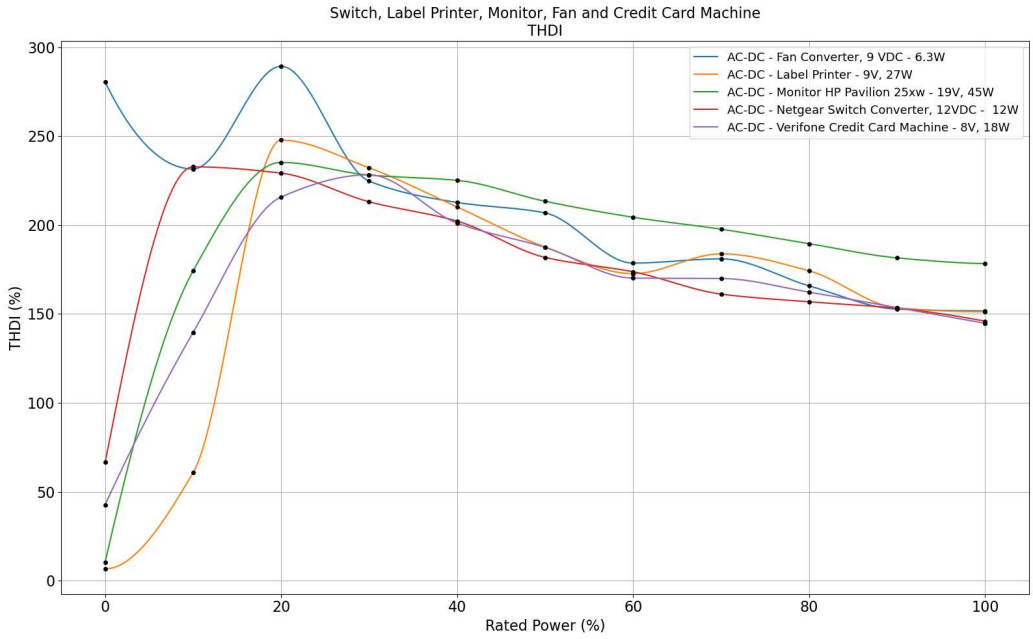


**Figure 4.7:** Switch, Label Printer, Monitor, Fan and Credit Card Machine - THDI.

## 4.3 Analysis

In general, the THDI generated by AC converters are uniformly high, with typical values for all converters above 100%. One way to mitigate this problem would be to use PFC in the converters, however cost is often an obstacle to its implementation [58–60].

The IEEE standard 519-2014 covers recommended practices and requirements for harmonic control in electric power systems, and requires cooperation between the utility and the users to maintain the current and voltage distortion below the limits. Although the utilities are responsible for providing a clean voltage signal to the customers, it is the customers' responsibility to not inject current harmonics above the permissible limits, otherwise they would be guilty as they are directly affecting the voltage distortion.

As we have seen, the highest current harmonic distortion generally occurred when the power converters were loaded 0-30% of rated capacity, and THDI decreased at higher power levels. This effect is known as harmonic attenuation, and significantly affects the magnitude and angle of harmonic components [36, 41]. While this work concentrates on current harmonics, in higher-impedance cabling systems, the I-R voltage can also cause voltage distortion.

Higher THDI might end up causing heating, electromagnetic interference and more losses in the power system. They can also cause errors in power metering, interference in telecommunication lines, and increase the current going back to the distribution transformer, increasing the wiring losses. Another effect on transformers is the increase of Eddy current losses. These are currents induced by magnetic flux in the transformer, which causes energy loss in its winding and core, and consequently more heating. The losses in the transformer due to eddy currents are proportional to the square of the current and the square of its frequency, so the higher the harmonic components, the higher the losses [56].

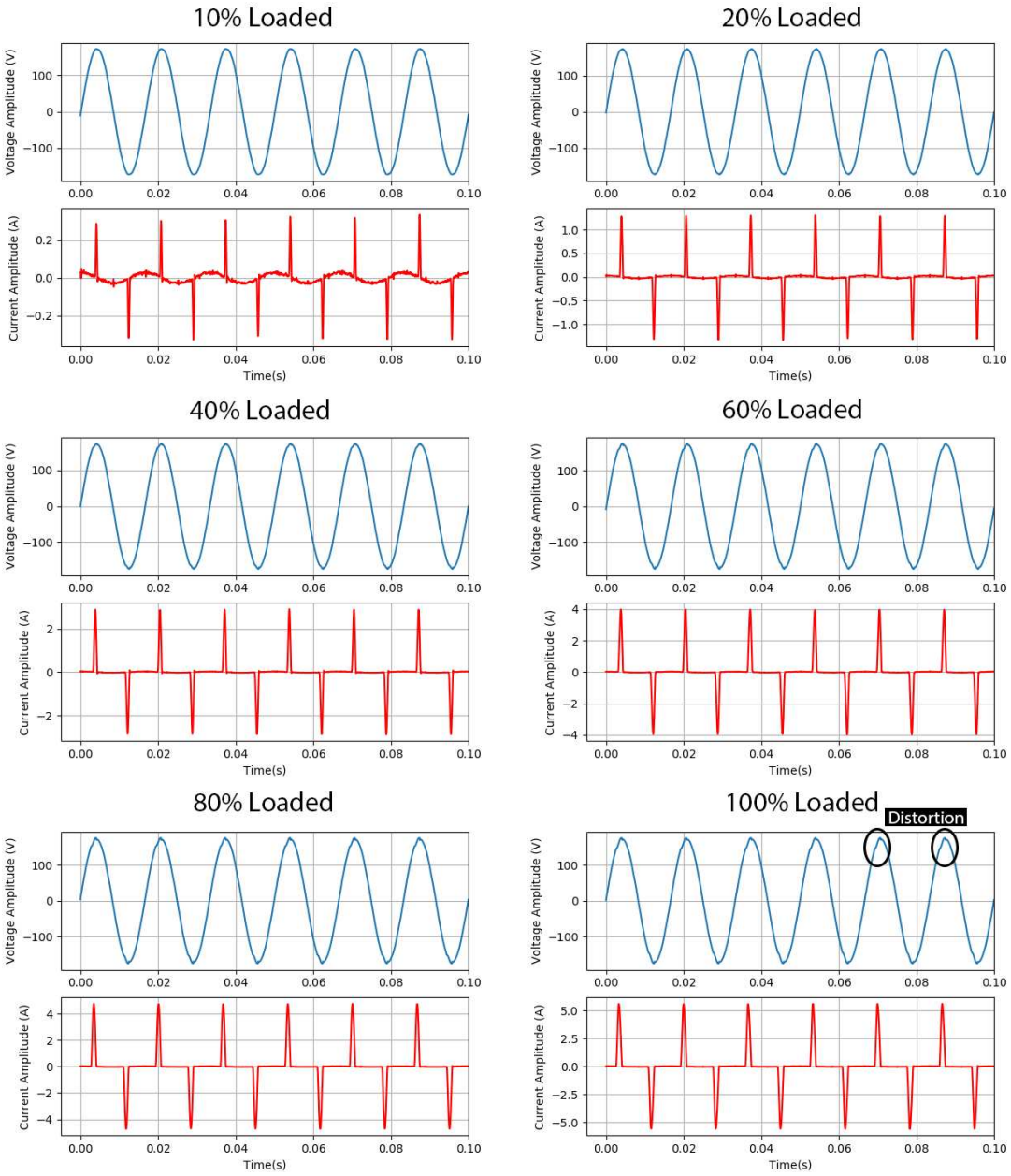


**Figure 4.8:** Laptop Charger - Harmonic Attenuation.

Although the current harmonics are greater at lower power levels, their absolute magnitude is lower compared to that of a harmonic at a higher power level, and therefore its effect on the distribution system is less. However, if there are several devices on the same network operating at low power levels, the harmonics may reinforce each other, increas-

ing losses. Such results are exemplified in an study made by Melo, Nuno et al., with measurements made in commercial electric vehicles [61].

Figure 4.8 shows the input current waveforms variations in power levels of an AC/DC HP laptop converter (18.5VDC, 90W). We can see that as the power levels change the current pulses; the less loaded the converter is, the smaller and narrower the pulse is. We can also see that the current waveforms become somewhat more sinusoidal as power increases (less harmonics). This is because as more power is used, the smooth capacitor discharges for a longer period in the load, therefore needing more energy and charging for a longer period. This causes the current pulse to be wider and closer to a sine wave, decreasing high order harmonics.

Additionally, in the bottom right of the figure, it is possible to see some voltage distortion. That tends to increase as the magnitude of the current harmonics increase or, in an aggregate power electronic device system, when harmonics interact with each other and the supply system impedance, causing voltage distortion.

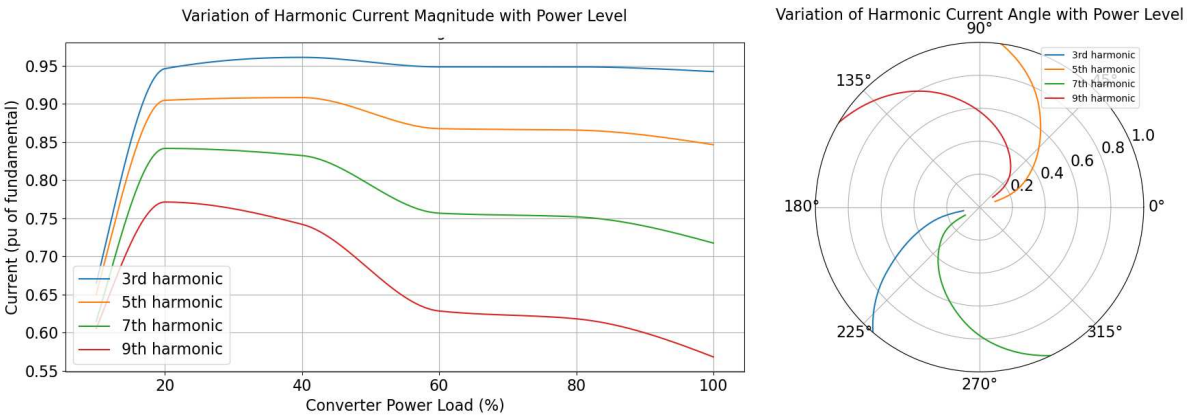


**Figure 4.9:** Laptop Charger Harmonic Current Attenuation. On the left the variation of harmonic current magnitude with power level. On the right, the variation of harmonic current angle with power level.

Figure 4.9 shows the variations in current harmonic magnitude and angle with power level. Higher harmonics have a higher attenuation with an increase in power level. Re-

garding the phase angles, the variations are also higher for higher harmonics, which means there's great potential for harmonic cancellation if other loads on the same circuit are operating at different power levels.

### 4.3.1 Harmonic Cancellation Experiments

Analyzing figure 4.9, it was found that the angular variation for the current harmonic components over the converter different power levels, presents a chance of cancellation among them, in case there is more than a converter connected to the same electrical circuit. The wider the angle diverges, the better the potential for cancellation. To investigate this hypothesis in more detail, two simulations were developed with laptops and screens, as these are loads commonly found in an office environment.

The *Simulation One* considered two laptop chargers, at different power levels, connected on the same circuit. The simulation compares the individual THDI values of each converter with the total THDI value present in the circuit and evaluates whether there was harmonic cancellation and how great it was.

In the *Simulation Two* , 3 different scenarios were considered. The scenarios were built under different types of loads and considered different ranges for the power levels in order to address real-world situations, and also the highest potential for harmonic cancellation if the loads operate in their full power range. The harmonic cancellation is measured through the Diversity Factor, which is explained in details in subsection 4.3.3.

### 4.3.2 Harmonic Cancellation - Simulation One

The purpose of this simulation is to detect current harmonic cancellation among two laptop converters connected to the same circuit, and at what power levels the lowest THDI is achieved.

The converter used for this analysis was the same one used previously in this section (AC/DC HP laptop converter, 18.5VDC, 90W). Testing provided (see Chapter 2) the magnitude and angle values for all current harmonic components (up to the 128th order) for

all power levels, varying from 0 to 100% of the rated power, in steps of 10%. When tests were run, these data was recorded in a *.csv file and was read by a python script, which is able to recreate the original AC current signal by summing the sinusoidal signals of each harmonic.

This simulation investigates harmonic cancellation when 2 identical converters are connected to the same circuit. For the first converter, the current signals for all power levels were stored in the variable *Signal Laptop* 1 represented by matrix A in equation 4.1 below. For the second converter, the data was stored in *Signal Laptop* 2, represented by matrix B. The sum of both signals, *Sum of Signals*, is represented by matrix C. The sum demonstrates different combinations of power levels between the two converters. In the equations below, for each current harmonic component, $k$ represents its order, $I_k$ the magnitude and $\theta_k$ the phase angle.

$$\begin{aligned} A = [&\sum_{k=0}^{128} I_k sin(2\pi k60t + \theta_k)\ at\ 0\%\ of\ rated\ power, \\ &\sum_{k=0}^{128} I_k sin(2\pi k60t + \theta_k)\ at\ 10\%\ of\ rated\ power, \\ &... \\ &\sum_{k=0}^{128} I_k sin(2\pi k60t + \theta_k)\ at\ 100\%\ of\ rated\ power] \end{aligned} \tag{4.1}$$

$$\begin{aligned} B = [&\sum_{k=0}^{128} I_k sin(2\pi k60t + \theta_k)\ at\ 0\%\ of\ rated\ power, \\ &\sum_{k=0}^{128} I_k sin(2\pi k60t + \theta_k)\ at\ 10\%\ of\ rated\ power, \\ &... \\ &\sum_{k=0}^{128} I_k sin(2\pi k60t + \theta_k)\ at\ 100\%\ of\ rated\ power] \end{aligned} \tag{4.2}$$

$$
\begin{aligned}
C = [&A_{1x1} + B_{1x1},\ A_{1x1} + B_{1x2},\ ...,\ A_{1x1} + B_{1x11},\\
&A_{1x2} + B_{1x1},\ A_{1x2} + B_{1x2},\ ...,\ A_{1x2} + B_{1x11},\\
&...\\
&A_{1x11} + B_{1x1},\ A_{1x11} + B_{1x2},\ ...,\ A_{1x11} + B_{1x11}]
\end{aligned}
\tag{4.3}
$$

The THDI was calculated for each element of matrices A, B and C. The results are depicted in Figure 4.10, where the top chart represents the THDI for each signal and the bottom chart represents the power level for each laptop. Every combination of laptop 1 and 2 was given an index number, starting from 0 up to 120 in order to encompass the total 121 possible combinations.

The THDI for the *Sum of Signals* is always less or equal to the highest THDI of one of the two laptop signals, proving that the distortion could be lower if we have two devices on the same network. For some combinations, the THDI for the *Sum of Signals* can be even lower than the THDI of both laptop signals, representing even better harmonic component cancellation.

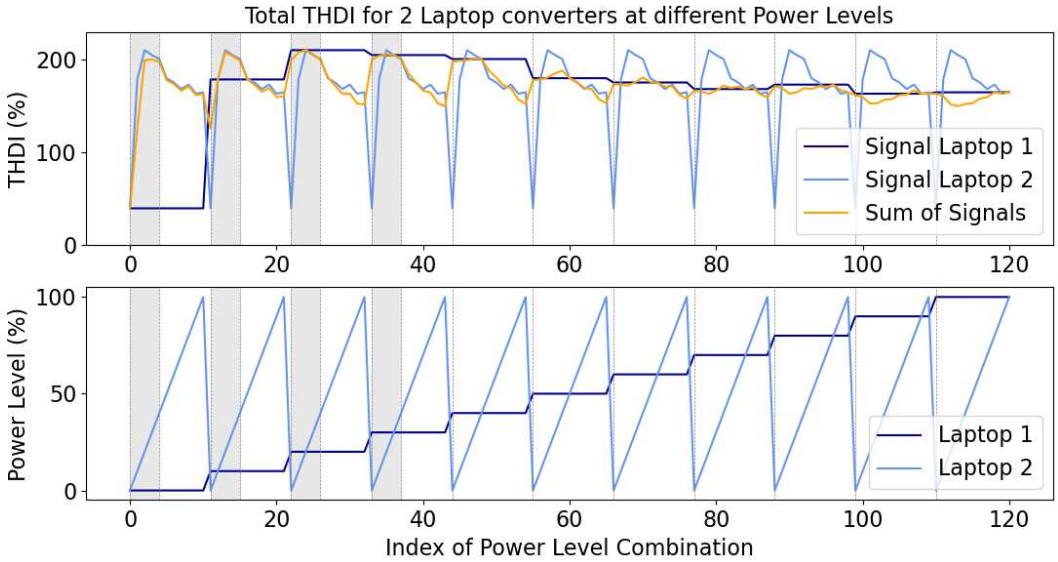


**Figure 4.10:** Total THDI for 2 Laptop Converters at Different Power Levels.

Chapter 3 presented data on the power range of many appliances, including laptop chargers. It was found that these devices operate below 40% of their capacity most of the time, with the majority never going above this level. The gray shaded areas on the chart represent the scenarios in which both converters are operating between 0-40% of power range.

Figure 4.11 shows combinations between both laptop converters power levels when the *Sum of Signals* THDI is lower than both signals' THDI individually. The best case scenario, where the highest harmonic cancellation is achieved, is when one converter is loaded at 30% and the other at 100%. Under those conditions, the *Sum of Signals* THDI is around 8% better than the lowest THDI of the signals.

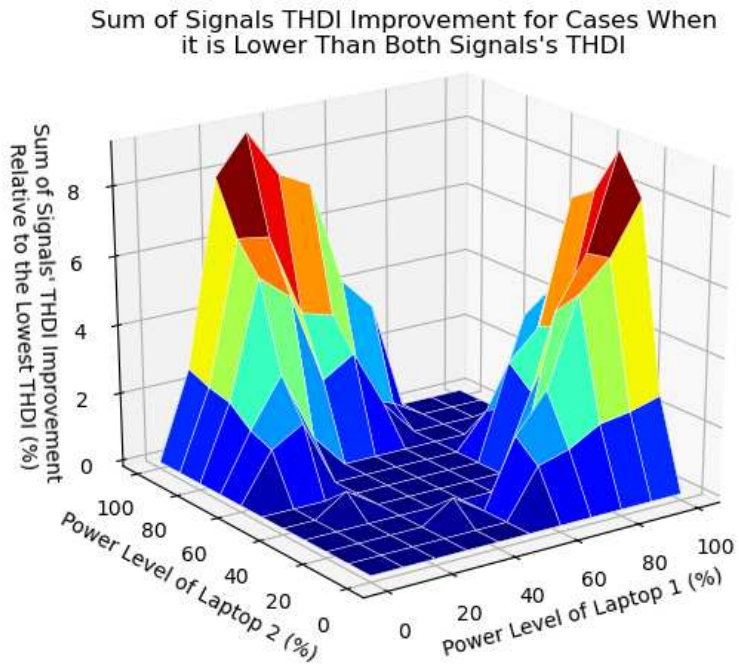


**Figure 4.11:** Sum of Signals' THDI improvement for cases when it is lower than both signals THDI.

On the other hand, when the converters are both loaded in the range of 0-50%, which comprises the most common operating range in the real world, we have the worst case scenarios for harmonic cancellation: the only time the Sum of Signals THDI was lower than the individual signals THDI, it was only 0.6% better. Therefore, in the operational power range of 0-40% found in Chapter 3 current harmonic cancellation still occurs, but not at the levels seen when one of the converters is operating near 100% load.

### 4.3.3 Harmonic Cancellation - Simulation 2

From section 4.3, we know that power level directly interacts with the phase angle dispersion of individual current harmonics. This simulation investigated how the harmonic cancellation behaves among many loads connected in parallel, operating at different power levels. Studies suggest that the quantification of this phase angle dispersion can be done through a factor defined as Current Harmonics Diversity Factor (DF) [33,36,47]:

$$DF_k = \frac{Magnitude\ of\ phasor\ sum\ of\ currents\ of\ harmonic\ k}{Magnitude\ of\ algebraic\ sum\ of\ currents\ of\ harmonic\ k} = \left| \frac{\sum_{k=1}^{N} I_k^i}{\sum_{k=1}^{N} \left| I_k^i \right|} \right| \tag{4.4}$$

$$I_k^i = \left| I_k^i \right| \angle \theta_k^i \tag{4.5}$$

$DF_k$ will range between 0 and 1; if it is closer to 1 it means the amount of harmonic cancellation was low, while if it is closer to 0, there was a significant amount of cancellation among the loads. Figure 4.12 shows 2 examples where DF was calculated for two signals at a frequency of 60Hz. The top chart shows a scenario where the cancellation was high and the DF is closer to 0, and the bottom chart shows one where the cancellation is low and the DF is closer to 1.

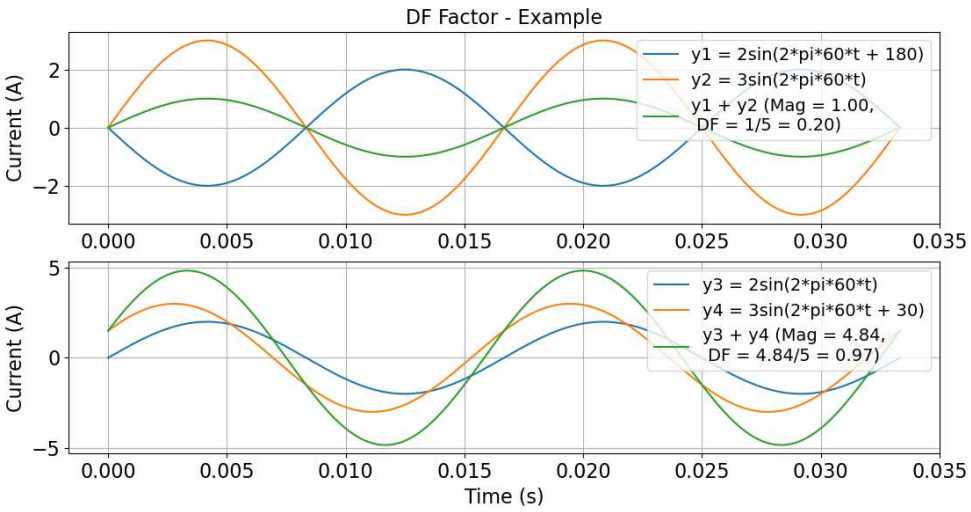


**Figure 4.12:** DF Factor - Example.

A Monte Carlo Simulation was implemented for three different scenarios. For each scenario, harmonic components (3rd, 5th, 7th, 9th, 11th, and 13th order) were analyzed when the distribution system had different numbers of devices connected in parallel. Each quantity of converters was analyzed using 1000 Monte Carlo iterations. The mean DF the 95% empirical confidence interval was extracted from the iterations. The three scenarios are explained below in details.

**Scenario 1**

In this scenario, the simulation considered 5, 10, 15, 20, 25, 30, and 35 laptop converters connected in parallel, a configuration similar to that of a large office complex. From measurements done in the laboratory, we have harmonic data for 9 different laptop converters, using the full range of their rated power when they are on (10% to 100%). Hence, for every iteration, harmonic data were randomly selected from the 9 laptop converters, and further randomized by choosing the power level for each laptop from a uniform distribution. Finally, the mean and the 95% confidence interval of the current DF were recorded. The results are shown in Figure 4.13.

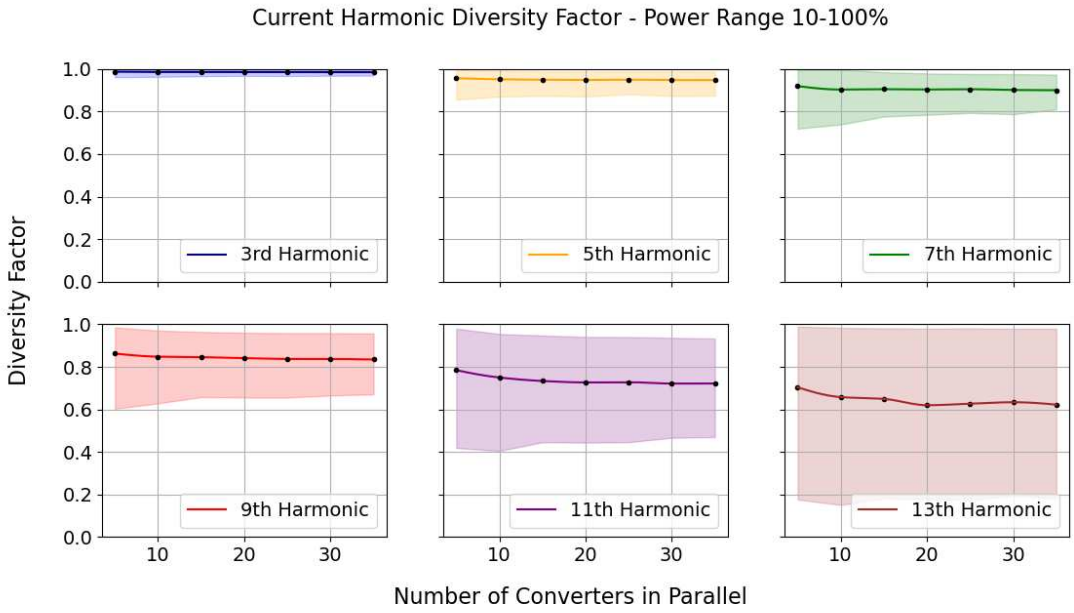


**Figure 4.13:** Scenario 1: Current harmonic diversity factor - Laptop converters with power range of 10-100%.

The results show that the most substantial harmonic cancellation occurred in the higher harmonics, as expected, since their current angles have higher variation. It can also be observed that as the harmonic order increases, so does the confidence interval width, indicating that harmonic cancellation varies widely with the randomly-selected load levels of the converters. Additionally, as more devices are added to the network, the total current distortion tends to decrease due to an increase in the harmonic cancellation.

However, in Chapter 3, it is shown that the operational power range of appliance converters significantly below rated power, with some devices never reaching above 60%. In the case of laptops, most of them operate below 20% of rated power most of the time. Taking this factor into account, another simulation was done for Scenario 2.

**Scenario 2**

In this scenario, all the parameters from Scenario 1 remain the same except for the converters' operational range. As shown in Figure 3.8, the majority of laptop converters operate 0-40% of rated power. Therefore, for this scenario to reflect a more realistic case,

we picked the power level distribution of the laptop connected to WEMO 2 (DELL Laptop Inspiron, with AC/DC converter model LA45NM140, 45W). As we have data at each 10% load step, Table 4.1 shows an approximation for the power level distribution when this device was on.

**Table 4.1:** DELL Laptop Inspiron, 45W (WEMO 2) - Power Level Distribution

| Power Level (%) | Probability (%) |
|---|---|
| 10 | 19.1 |
| 20 | 48.6 |
| 30 | 13.3 |
| 40 | 8.29 |
| 50 | 4.13 |
| 60 | 3.01 |
| 70 | 1.83 |
| 80 | 0.95 |
| 90 | 0.32 |
| 100 | 0.47 |

Approximately 90% of the time the converters are operating at 10-40% of their nominal capacity. Figure 4.14 depicts the results for this scenario.

In this case, we still see better harmonic cancellation for high order harmonics. However, the DF for harmonic components is higher when compared to the previous results – i.e. less cancellation. If we take the DF values for the 13th harmonic for example, its lowest value in the Scenario 1 is close to 0.6, but in Scenario 2 it is 0.8. Also, looking at the 95% confidence interval for the 13th, it shows a narrower potential for harmonic cancellation, compared with the results from Scenario 1. This indicates that there is substantially less harmonic cancellations when using actual load levels compared to simulations using randomly selected loads spanning the rated capacity of the converters. It doesn't show, however, the cancellation effect among a diversity of devices.

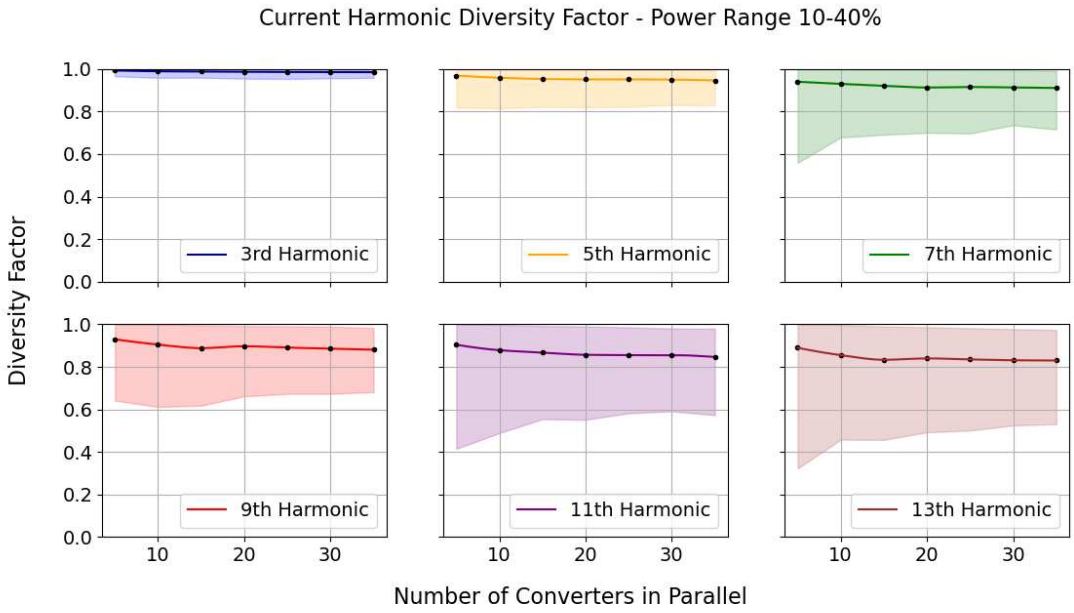


**Figure 4.14:** Scenario 2: Current harmonic diversity factor - Laptop converters with realistic power range of 10-40%.

### Scenario 3

This last scenario considered heterogeneous devices operating at realistic load levels, as it is more representative of an office environment. The simulation considered 4, 10, 14, 20, 24, 30, and 34 devices connected in parallel, composed half of laptops and half screens. The laptop converter harmonics data was randomly selected among the 9 converters tested in the lab, and the power level distribution was the same used in Scenario 2 (Table 4.1). For the screens, we collected harmonic data from three different screen models in the lab (HP Model 273, HP EliteDisplay E232, HP EliteDisplay E242). For each model, three different power levels were considered when they were on: with black screen, white screen, and playing a video. The screen power levels were randomly selected in a uniform distribution.

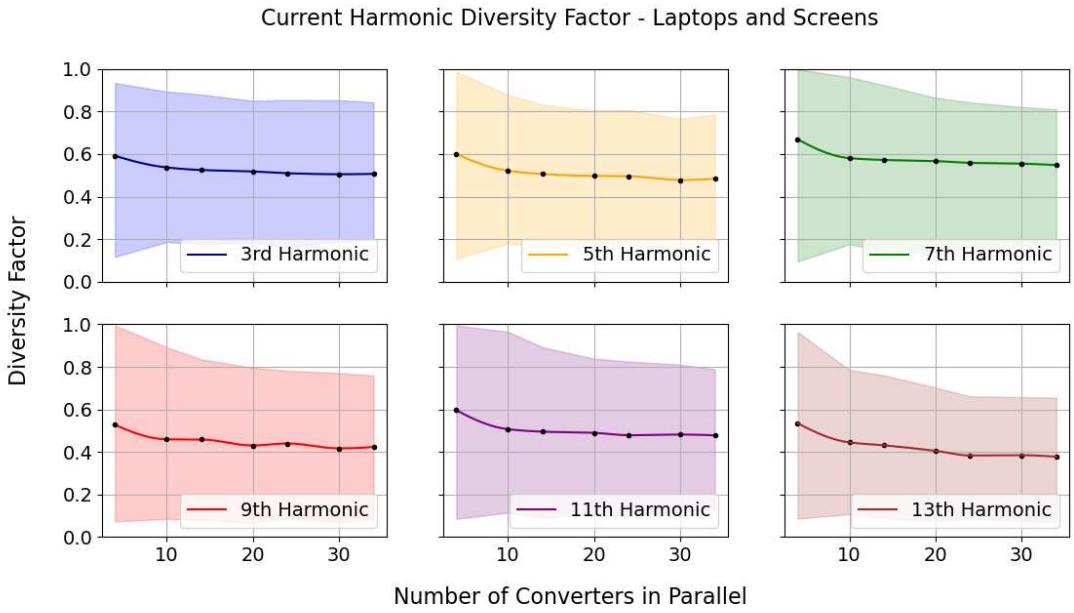


**Figure 4.15:** Scenario 3: Current harmonic diversity factor - Laptops converters and screens at realistic power ranges.

Figure 4.15 shows the mean and the 95% confidence interval of the current DF recorded. While in Scenarios 1 and 2, the confidence interval was wide only for high harmonics, in this case, we perceive a wider confidence interval also for the low harmonics. This is explained by the greater variety of current waveforms, which when added together in the various possible scenarios, present more dispersed results. This dispersion, as observed in the other scenarios, tends to decrease with the quantity of loads connected to the circuit.

To illustrate the variety of waveforms, figure 4.16 shows one possible scenario where one of the laptops is 20% loaded and one of the screens is on with a black screen.

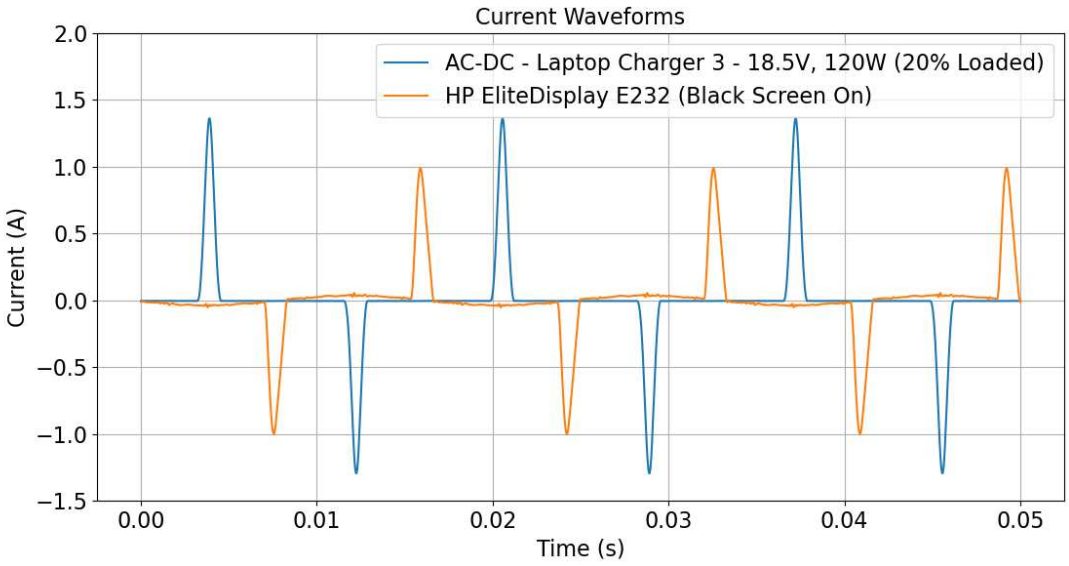


**Figure 4.16:** Laptop and Screen - Current Waveforms.

For Scenario 3, the cancellation was considerably higher when compared to Scenario 1 and 2, and the DF of the lower order harmonics, such as the 3rd, 5th and 7th had a significant drop, which did not happen in the two previous scenarios. If we consider the mean of the DF for all devices in parallel, the 3rd harmonic cancellation was 46.4% and 46.5% higher, when compared to Scenarios 1 and 2 respectively. For the 5th order component, harmonic cancellation increased by 46.1% and 46.3% respectively, and for the 7th 36.1% and 37.1%. The third harmonic exhibited even 8.8% higher harmonic cancellation than the high-order 7th component, different from what had been observed so far, where higher order harmonics had always presented lower DF (higher cancellation). This can be explained by the non-coincidence of the peaks of the current waveforms, which allowed a wider range for cancellation.

At the end of this thesis, in Appendix B, there are the tables containing all DF values for these three scenarios.

# Chapter 5

# Conclusion

In this work, a testbed was set up to support systematic data collection of power system characteristics of converters and appliances. This physical setup contributed to later phases of the project, where the modeling of the analyzed equipment operating in AC and DC was made, a fundamental tool in the development of the DC Design and Scope Tool. The test bed was also utilized to compare AC and DC power distribution systems, which will be covered in subsequent papers. Test results supported a robust analysis of the generation of harmonics in AC systems by AC/DC converters common to MELs.

Based on the analyses performed, factors that directly influence harmonic injection in low voltage AC distribution systems are: the operating power range of the electronic converters, the number of devices connected in parallel on one circuit, the diversity of the devices/converters, and the impedance of the system supply interacting with the current harmonics, which will cause more or less voltage distortion.

We have also seen that AC/DC converters for appliances commonly found in an office environment (phone chargers, laptops, printers, screens and network devices) operate, for the majority of the time they are powered on, at below 40% of their nominal power. This operating power range coincides with the interval in which highest levels of current harmonics are injected into the electrical system.

Despite that, the presence of several converters on the same network favors the cancellation of current harmonic components, especially higher order components. While low order current components present little diversity in phase angle with a change in load level, higher harmonics present bigger variations, increasing the potential for cancellation. This harmonic cancellation is stronger when the converters in the system have a greater variation in power level and when different types of converters (manufacturers and power levels) are loading the same circuit.

## 5.1 Future Work

It has been determined that harmonics could cause problems in the power system. A distribution network generally has different non-linear loads connected to it, which can result in different harmonic patterns and rate of harmonic cancellation. Future investigations are recommended with additional scenarios where more types of converters are connected to the same network, with different power distribution profiles.

Another problem related to harmonics is the loss of efficiency in transformers from current harmonics. For example, the choice of transformer may have substantial impact on the transformer's dissipation of harmonic components. The initial construction of the testbed included a 3kVA $\Delta - Y$ transformer, and based upon price, a Dayton model 44YV25 was purchased. However, during characterization, the transformer's behavior did not match that of a $\Delta - Y$ transformer, and further investigation revealed that it was a low cost variant with fewer windings called a 'Scott-T', operating in a T-to-T arrangement. This type of transformer is composed of two single phase transformers which, depending on the way they are connected, allows for a three-phase to three-phase connection arrangement. For cost-savings reasons, this type of transformer is widely used for low power systems. However, the literature cites some disadvantages of this configuration, such as lower voltage stability, bigger size and heavier weight when compared to a regular three-phase transformer [56, 62, 63]. While full characterization could not be performed at the time, initial results indicated that the harmonic absorption of this type of transformer differs substantially from that of a true $\Delta - Y$ configuration. Therefore, an option for future work would be the characterization of both transformer types, and comparison of their performance with a high-harmonic load.

A third topic for investigation would be to use the data collected by the WEMOs to estimate DC power consumption, supposing that the appliances were connected to DC/DC converters. It would be possible to calculate the net efficiency for the appliances operat-

ing in AC and also in DC, and then do a comparison between AC and DC low voltage distribution systems, regarding only the end point of use.

# Bibliography

[1] Venkata Anand Prabhala, Bhanu Prashant Baddipadiga, Poria Fajri, and Mehdi Ferdowsi. An overview of direct current distribution system architectures & benefits. *Energies*, 11(9):2463, 2018.

[2] Laurens Mackay, Nils H van der Blij, Laura Ramirez-Elizondo, and Pavol Bauer. Toward the universal dc distribution system. *Electric Power Components and Systems*, 45(10):1032–1042, 2017.

[3] Annabelle Pratt, Pavan Kumar, and Tomm V Aldridge. Evaluation of direct current distribution in data centers to improve energy efficiency. *The Data Center Journal*, 28, 2007.

[4] Annabelle Pratt, Pavan Kumar, and Tomm V Aldridge. Evaluation of 400v dc distribution in telco and data centers to improve energy efficiency. In *INTELEC 07-29th International Telecommunications Energy Conference*, pages 32–39. IEEE, 2007.

[5] A. F. B. Santos, G. P. Duggan, C. D. Lute, and D. J. Zimmerle. An efficiency comparison study for small appliances operating in dc and ac in minigrids. In *2018 IEEE Global Humanitarian Technology Conference (GHTC)*, pages 1–2, Oct 2018.

[6] Roberto Rudervall, JP Charpentier, Raghuveer Sharma, et al. High voltage direct current (hvdc) transmission systems technology review paper. *Energy week*, 2000:1–19, 2000.

[7] Dakota Roberson, H Clarisse Kim, Bo Chen, Christine Page, Reynaldo Nuqui, Alfonso Valdes, Richard Macwan, and Brian K Johnson. Improving grid resilience using high-voltage dc: Strengthening the security of power system stability. *IEEE Power and Energy Magazine*, 17(3):38–47, 2019.

[8] Arthur Santos, James Cale, Avpreet Singh, et al. Comparison of load models for estimating electrical efficiency in dc microgrids. *The 3rd IEEE International Conference on DC Microgrids*, 2019.

[9] Arthur Felicio B Santos, Gerald P Duggan, Christopher D Lute, and Daniel J Zimmerle. An efficiency comparison study for small appliances operating in dc and ac in minigrids. In *2018 IEEE Global Humanitarian Technology Conference (GHTC)*, pages 1–2. IEEE, 2018.

[10] Venkata Anand Kishore Prabhala, Bhanu Prashant Baddipadiga, and Mehdi Ferdowsi. Dc distribution systemsâĂŤan overview. In *2014 International Conference on Renewable Energy Research and Application (ICRERA)*, pages 307–312. IEEE, 2014.

[11] Alexis Kwasinski. Evaluation of dc voltage levels for integrated information technology and telecom power architectures. In *4th International Telecommunication-Energy special conference*, pages 1–7. VDE, 2009.

[12] Dushan Boroyevich, Igor Cvetković, Dong Dong, Rolando Burgos, Fei Wang, and Fred Lee. Future electronic power distribution systems a contemplative view. In *2010 12th International Conference on Optimization of Electrical and Electronic Equipment*, pages 1369–1380. IEEE, 2010.

[13] Basile Margaritis and Peter Ide. Contemporary architectures for power systems considering future trends. 2001.

[14] Tero Kaipia, Pasi Salonen, Jukka Lassila, and Jarmo Partanen. Possibilities of the low voltage dc distribution systems. In *Proc. NORDAC 2006 conference, Stockholm*, 2006.

[15] Hiroaki Kakigano, Yushi Miura, and Toshifumi Ise. Low-voltage bipolar-type dc microgrid for super high quality distribution. *IEEE transactions on power electronics*, 25(12):3066–3075, 2010.

[16] Jianjun Ma, Yan Li, Miao Zhu, and Xu Cai. Parallel operation of distributed voltage balancers for bipolar dc system with improved reliability and efficiency. In *IECON 2017-43rd Annual Conference of the IEEE Industrial Electronics Society*, pages 1387–1392. IEEE, 2017.

[17] G. AlLee and W. Tschudi. Edison redux: 380 vdc brings reliability and efficiency to sustainable data centers. *IEEE Power and Energy Magazine*, 10(6):50–59, Nov 2012.

[18] Francisco Martin-Martínez, Alvaro Sánchez-Miralles, and M Rivier. A literature review of microgrids: A functional layer based classification. *Renewable and Sustainable Energy Reviews*, 62:1133–1153, 2016.

[19] Daniel L Gerber, Vagelis Vossos, Wei Feng, Chris Marnay, Bruce Nordman, and Richard Brown. A simulation-based efficiency comparison of ac and dc power distribution networks in commercial buildings. *Applied Energy*, 210:1167–1187, 2018.

[20] Vagelis Vossos, Stephen Pantano, Ruby Heard, and Rich Brown. Dc appliances and dc power distribution. *A Bridge to the Future Net Zero Energy Homes. Lawrence Berkeley National Laboratory (LBNL)*, 2017.

[21] Alexander Stippich, Alexander Sewergin, Georges Engelmann, Jan Gottschlich, Markus Neubert, Christoph van der Broeck, Philipp Schuelting, Rafael Goldbeck, and Rik De Doncker. From ac to dc: Benefits in household appliances. In *International ETG Congress 2017*, pages 1–6. VDE, 2017.

[22] Karina Garbesi, Vagelis Vossos, and Hongxia Shen. Catalog of dc appliances and power systems. Technical report, Lawrence Berkeley National Lab.(LBNL), Berkeley, CA (United States), 2010.

[23] M Jawad Ghorbani and Hossein Mokhtari. Impact of harmonics on power quality and losses in power distribution systems. *International Journal of Electrical & Computer Engineering (2088-8708)*, 5(1), 2015.

[24] A Elmoudi, M Lehtonen, and Hasse Nordman. Effect of harmonics on transformers loss of life. In *Conference Record of the 2006 IEEE International Symposium on Electrical Insulation*, pages 408–411. IEEE, 2006.

[25] Yang Wang, Jing Yong, Yuanyuan Sun, Wilsun Xu, and Daniel Wong. Characteristics of harmonic distortions in residential distribution systems. *IEEE Transactions on Power Delivery*, 32(3):1495–1504, 2016.

[26] Arshad Mansoor. Lower order harmonic cancellation: impact of low-voltage network topology. In *IEEE Power Engineering Society. 1999 Winter Meeting (Cat. No. 99CH36233)*, volume 2, pages 1106–1109. IEEE, 1999.

[27] J Carlos Gómez and Medhat M Morcos. Impact of ev battery chargers on the power quality of distribution systems. *IEEE transactions on power delivery*, 18(3):975–981, 2003.

[28] Jan JM Desmet, Isabel Sweertvaegher, Greet Vanalme, Kurt Stockman, and Ronnie JM Belmans. Analysis of the neutral conductor current in a three-phase supplied network with nonlinear single-phase loads. *IEEE Transactions on Industry Applications*, 39(3):587–593, 2003.

[29] M Davudi, S Torabzad, and B Ojaghi. Analysis of harmonics and harmonic mitigation methods in distribution systems. *Australian Journal of Basic and Applied Sciences*, 5(11):996–1005, 2011.

[30] Lauri Kütt, Eero Saarijärvi, Matti Lehtonen, Heigo Mõlder, and Jaan Niitsoo. A review of the harmonic and unbalance effects in electrical distribution networks due to ev charging. In *2013 12th International Conference on Environment and Electrical Engineering*, pages 556–561. IEEE, 2013.

[31] Raneru Nageswara Rao. Harmonic analysis of small scale industrial loads and harmonic mitigation techniques in industrial distribution system. *International Journal of Engineering Research and Applications*, 3(4):1511–1540, 2013.

[32] Josep Balcells and Josep García. Impact of plug-in electric vehicles on the supply grid. In *2010 IEEE Vehicle Power and Propulsion Conference*, pages 1–4. IEEE, 2010.

[33] Sasa Z Djokic and Adam J Collin. Cancellation and attenuation of harmonics in low voltage networks. In *2014 16th International Conference on Harmonics and Quality of Power (ICHQP)*, pages 137–141. IEEE, 2014.

[34] Jan Meyer, Peter Schegner, and Kurt Heidenreich. Harmonic summation effects of modern lamp technologies and small electronic household equipment. In *Proc. 21st International. Conf. on Electricity Distribution (CIRED)*, 2011.

[35] V Ćuk, JFG Cobben, WL Kling, and RB Timens. An analysis of diversity factors applied to harmonic emission limits for energy saving lamps. In *Proceedings of 14th International Conference on Harmonics and Quality of Power-ICHQP 2010*, pages 1–6. IEEE, 2010.

[36] A Mansoor, WM Grady, AH Chowdhury, and MJ Samotyi. An investigation of harmonics attenuation and diversity among distributed single-phase power electronic loads. In *Proceedings of IEEE/PES Transmission and Distribution Conference*, pages 110–116. IEEE, 1994.

[37] Matthew Rylander, W Mack Grady, and Martin Narendorf. Experimental apparatus, testing results, and interpretation of the impact of voltage distortion on the current distortion of typical single-phase loads. *IEEE transactions on power delivery*, 24(2):844–851, 2009.

[38] Paulo Fernando Ribeiro. *Time-varying waveform distortions in power systems*, volume 6. John Wiley & Sons, 2009.

[39] PF Ribeiro. *Investigations of harmonic penetration in transmission systems*. PhD thesis, 1985.

[40] João P Trovão, Paulo G Pereirinha, Leonor Trovão, and Humberto M Jorge. Electric vehicles chargers characterization: Load demand and harmonic distortion. In *11th International Conference on Electrical Power Quality and Utilisation*, pages 1–7. IEEE, 2011.

[41] A Mansoor, WM Grady, RS Thallam, MT Doyle, SD Krein, and MJ Samotyj. Effect of supply voltage harmonics on the input current of single-phase diode bridge rectifier loads. *IEEE Transactions on Power Delivery*, 10(3):1416–1422, 1995.

[42] Hussein A Attia, M El-Metwally, and Osama M Fahmy. Harmonic distortion effects and mitigation in distribution systems. *Journal of American Science*, 6(10):173–183, 2010.

[43] A Mansoor, WM Grady, PT Staats, RS Thallam, MT Doyle, and MJ Samotyj. Predicting the net harmonic currents produced by large numbers of distributed single-phase computer loads. *IEEE Transactions on Power Delivery*, 10(4):2001–2006, 1995.

[44] W Mack Grady, Arshad Mansoor, Ewald F Fuchs, Paola Verde, and Michael Doyle. Estimating the net harmonic currents produced by selected distributed single-phase loads: computers, televisions, and incandescent light dimmers. In *2002 IEEE Power Engineering Society Winter Meeting. Conference Proceedings (Cat. No. 02CH37309)*, volume 2, pages 1090–1094. IEEE, 2002.

[45] A Mansoor and WM Grady. Analysis of compensation factors influencing the net harmonic current produced by single-phase nonlinear loads. In *8th International Conference on Harmonics and Quality of Power. Proceedings (Cat. No. 98EX227)*, volume 2, pages 883–889. IEEE, 1998.

[46] YG Hegazy and MMA Salama. Calculations of diversified harmonic currents in multiple converter systems. In *2000 Power Engineering Society Summer Meeting (Cat. No. 00CH37134)*, volume 2, pages 727–731. IEEE, 2000.

[47] Adam J Collin, Charles E Cresswell, and Saša Ž Djokic. Harmonic cancellation of modern switch-mode power supply load. In *Proceedings of 14th International Conference on Harmonics and Quality of Power-ICHQP 2010*, pages 1–9. IEEE, 2010.

[48] Department of Energy of the United States. Energy design and scoping tool for dc distribution systems. https://www.energy.gov/eere/buildings/downloads/energy-design-and-scoping-tool-dc-distribution-systems, 2017. Accessed: 2020-04-23.

[49] Rich Brown, Vagelis Vossos, Daniel Gerber, Stephen M Frank, and Lester Shen. Making better use of on-site pv generation: Direct distribution of dc power in buildings. Technical report, National Renewable Energy Lab.(NREL), Golden, CO (United States), 2020.

[50] Mack Grady. Understanding power system harmonics. *Austin, TX: University of Texas*, 2006.

[51] Display specifications. https://www.displayspecifications.com/. Accessed: 2020-05-10.

[52] DellâĎć e2010h/e2210h/e2310h flat panel monitor user's guide. https://gzhls.at/blob/ldb/1/c/7/2/c90bce1524fee3a44c71a7d9dbd81a7f03f9.pdf. Accessed: 2020-05-10.

[53] Hp officejet pro 9018 all-in-one printer. http://content.etilize.com/Manufacturer-Brochure/1060292677.pdf. Accessed: 2020-05-10.

[54] Hp laserjet 1022. http://h10032.www1.hp.com/ctg/Manual/c00264442. Accessed: 2020-05-10.

[55] Netgeat - readynas 300/500/700 series network attached storage (nas). http://www.downloads.netgear.com/files/GDC/datasheet/en/RN300-RN500-RN700.pdf. Accessed: 2020-05-10.

[56] Roger C Dugan, Mark F Mc Granaghan, Surya Santoso, and H Wayner Beaty. Electric power systems quality, 2004.

[57] Design a switch mode power supply using an isolated flyback topology. https://www.digikey.com/en/articles/design-switch-mode-power-supply-isolated-flyback-topology. Accessed: 2020-06-10.

[58] Haruo Watanabe, Yoshinori Kobayashi, Yutaka Sekine, MAMM Morikawa, and TAIT Ishii. The suppressing harmonic currents, ms (magnetic-switch) power supply. In *Proceedings of INTELEC 95. 17th International Telecommunications Energy Conference*, pages 783–790. IEEE, 1995.

[59] Fu-Sheng Tsai, P Markowski, and E Whitcomb. Off-line flyback converter with input harmonic current correction. In *Proceedings of Intelec'96-International Telecommunications Energy Conference*, pages 120–124. IEEE, 1996.

[60] Jong-Jae Lee, Jung-Min Kwon, Eung-Ho Kim, Woo-Young Choi, and Bong-Hwan Kwon. Single-stage single-switch pfc flyback converter using a synchronous rectifier. *IEEE Transactions on Industrial Electronics*, 55(3):1352–1365, 2008.

[61] Nuno Melo, Francisco Mira, Aníbal de Almeida, and Joaquim Delgado. Integration of pev in portuguese distribution grid: Analysis of harmonic current emissions in charging points. In *11th International Conference on Electrical Power Quality and Utilisation*, pages 1–6. IEEE, 2011.

[62] Alceu Andre Badin and Ivo Barbi. Three-phase series-buck rectifier with split dc-bus based on the scott transformer. In *2008 IEEE Power Electronics Specialists Conference*, pages 516–522. IEEE, 2008.

[63] Yasuko Aihara, Ryo Miyazawa, and Hirotaka Koizumi. A study on the effect of the scott transformer on the three-phase unbalance in distribution network with single-phase generators. In *2012 3rd IEEE International Symposium on Power Electronics for Distributed Generation Systems (PEDG)*, pages 283–290. IEEE, 2012.

# Appendix A

# Python Codes

**Controllable Load Bank Python Code**

In order to test the multiple values of resistance, a python code was written. Although it is possible to have 256 different values of resistance with this configuration, the code below has the purpose of finding 10 appropriate resistance values between 0W and the converter under test's rated power, and execute the following functions in this particular order:

1. Variate increasingly from the minimum power to its rated power.
2. Variate decreasingly from its rated power to the minimum power.
3. Make random variations of power, within the range of rated and minimum power.

The code has a Graphic User Interface, so the user can insert values of the voltage and rated power of the converter being test. With those values, it calculates what resistors in the load bank should be combined to achieve the appropriate resistance value and perform the test in the correct order. The code to find the resistors arrangement can be found here: https://hdl.handle.net/10217/207807

# Appendix B

# Simulation 2 - Tables for Current Harmonic Diversity Factor

Below are the tables for the three scenarios considered in Chapter 4, Simulation 2.

**Table B.1:** Scenario 1 - Current Harmonic Diversity Factor

| Scenario 1 | | | | | | |
|---|---|---|---|---|---|---|
| Devices in Parallel | Harmonic Order | | | | | |
| | 3 | 5 | 7 | 9 | 11 | 13 |
| 5 | 0.9871 | 0.9564 | 0.9194 | 0.8624 | 0.7846 | 0.7041 |
| 10 | 0.9858 | 0.9515 | 0.9032 | 0.8480 | 0.7501 | 0.6580 |
| 15 | 0.9858 | 0.9493 | 0.9050 | 0.8456 | 0.7337 | 0.6494 |
| 20 | 0.9854 | 0.9482 | 0.9034 | 0.8411 | 0.7270 | 0.6199 |
| 25 | 0.9851 | 0.9497 | 0.9048 | 0.8371 | 0.7280 | 0.6269 |
| 30 | 0.9844 | 0.9479 | 0.9012 | 0.8371 | 0.7216 | 0.6339 |
| 35 | 0.9849 | 0.9475 | 0.9001 | 0.8347 | 0.7219 | 0.6223 |

**Table B.2:** Scenario 2 - Current Harmonic Diversity Factor

| Scenario 2 | | | | | | |
|---|---|---|---|---|---|---|
| Devices in Parallel | Harmonic Order | | | | | |
| | 3 | 5 | 7 | 9 | 11 | 13 |
| 5 | 0.9929 | 0.9687 | 0.9398 | 0.9297 | 0.9040 | 0.8896 |
| 10 | 0.9892 | 0.9586 | 0.9299 | 0.9048 | 0.8785 | 0.8552 |
| 15 | 0.9879 | 0.9529 | 0.9208 | 0.8881 | 0.8670 | 0.8333 |
| 20 | 0.9867 | 0.9508 | 0.9128 | 0.8970 | 0.8568 | 0.8398 |
| 25 | 0.9858 | 0.9511 | 0.9152 | 0.8906 | 0.8552 | 0.8352 |
| 30 | 0.9854 | 0.9500 | 0.9131 | 0.8856 | 0.8553 | 0.8312 |
| 35 | 0.9849 | 0.9459 | 0.9106 | 0.8808 | 0.8468 | 0.8301 |

**Table B.3:** Scenario 3 - Current Harmonic Diversity Factor

| Scenario 1 | | | | | | |
|---|---|---|---|---|---|---|
| Devices in Parallel | Harmonic Order | | | | | |
| | 3 | 5 | 7 | 9 | 11 | 13 |
| 5 | 0.5924 | 0.6011 | 0.6697 | 0.5280 | 0.5966 | 0.5358 |
| 10 | 0.5373 | 0.5214 | 0.5809 | 0.4597 | 0.5072 | 0.4451 |
| 15 | 0.5251 | 0.5064 | 0.5724 | 0.4588 | 0.4956 | 0.4314 |
| 20 | 0.5183 | 0.4972 | 0.5670 | 0.4307 | 0.4900 | 0.4055 |
| 25 | 0.5099 | 0.4961 | 0.5587 | 0.4401 | 0.4789 | 0.3837 |
| 30 | 0.5053 | 0.4780 | 0.5551 | 0.4170 | 0.4820 | 0.3850 |
| 35 | 0.5071 | 0.4843 | 0.5482 | 0.4243 | 0.4782 | 0.3779 |